Ridge segmentation and the magnetic structure of the Southwest Indian Ridge (at 50°30'E, 55°30'E and 66°20'E): Implications for magmatic processes at ultraslow-spreading centers.

Daniel Sauter, Hélène Carton, Véronique Mendel, Marc Munschy, Céline Rommevaux-Jestin, Jean-Jacques Schott, Hubert Whitechurch

Geochemistry Geophysics Geosystems G3
AN ELECTRONIC JOURNAL OF THE EARTH SCIENCES
Published by AGU and the Geochemical Society

Article
Volume 5, Number 5
14 May 2004
Q05K08, doi:10.1029/2003GC000581
ISSN: 1525-2027

Ridge segmentation and the magnetic structure of the Southwest Indian Ridge (at 50°30′E, 55°30′E and 66°20′E): Implications for magmatic processes at ultraslow-spreading centers

Daniel Sauter
Institut de Physique du Globe de Strasbourg, CNRS-ULP, 5 rue René Descartes, 67084 Strasbourg Cedex, France (daniel.sauter@eost.u-strasbg.fr)

Hélène Carton
Institut de Physique du Globe de Paris, CNRS-UPMC, 4 Place Jussieu, 75252 Paris Cedex 05, France (carton@ipgp.jussieu.fr)

Véronique Mendel and Marc Munschy
Institut de Physique du Globe de Strasbourg, CNRS-ULP, 5 rue René Descartes, 67084 Strasbourg Cedex, France (veronique.mendel@eost.u-strasbg.fr; marc.munschy@eost.u-strasbg.fr)

Céline Rommevaux-Jestin
Institut de Physique du Globe de Paris, CNRS-UPMC, 4 Place Jussieu, 75252 Paris Cedex 05, France (rommevau@ipgp.jussieu.fr)

Jean-Jacques Schott and Hubert Whitechurch
Institut de Physique du Globe de Strasbourg, CNRS-ULP, 5 rue René Descartes, 67084 Strasbourg Cedex, France (jeanjacques.schott@eost.u-strasbg.fr; hubert.whitechurch@eost.u-strasbg.fr)

[1] The aim of this paper is to investigate the relationships between the segmentation and the magnetic structure of the ultraslow-spreading Southwest Indian Ridge. Contrary to faster spreading ridges, magnetization usually decreases from high values along the neovolcanic axis to low values in the nontransform discontinuities. There is a direct correlation between the deepening of the axial valley and the decrease of the magnetization from the neovolcanic axis toward the deepest parts of the axial discontinuities. We suggest that less frequent eruptions as the distance from the segment center and the length of these discontinuities increase, result in thinner extrusive lavas and thus control the along-axis magnetization variations by thinning the magnetic source layer. A unique segment centered at 50°28′E shows a marked low magnetization anomaly at its center similarly to the segments of the slow-spreading Mid-Atlantic Ridge. We suggest that in this segment both the mantle temperature and the magmatic activity are high enough for the lavas not to be highly fractionated. A higher rate of melt production to the west of Gallieni transform fault may have created some form of reservoir where mixing of melts occurs and where crystalline fractionation is low producing low-magnetization lavas. To the east, magma chambers may be smaller with cooler mantle temperatures resulting in restricted mixing and significant fractionation which may lead to relatively high intensity magnetization lavas. Finally, we propose that serpentinization of peridotites has no significant contribution to the variation of the magnetization along the axial valley. Off-axis, in thin crust areas, upper mantle rocks may become progressively more altered, as distance from the axis increases. The strong faulting and alteration of a thin basaltic cap and underlying upper mantle rocks can produce the disappearance of the magnetic reversal pattern and the increase of the magnetization

which is observed along the traces of the largest amagmatic discontinuities. By contrast, in thicker crust areas, the upper mantle rocks are shielded from the alteration and the serpentinization process may be delayed resulting, as on the Mid-Atlantic Ridge, in slightly more positive magnetization values along the traces of axial discontinuities, regardless of polarity.

Components: 11,232 words, 14 figures.

Keywords: Mid-ocean ridges; Southwest Indian Ridge; crustal magnetization; ridge segmentation; ultraslow spreading.

Index Terms: 1550 Geomagnetism and Paleomagnetism: Spatial variations attributed to seafloor spreading (3005); 3035 Marine Geology and Geophysics: Midocean ridge processes; 3045 Marine Geology and Geophysics: Seafloor morphology and bottom photography; 9340 Information Related To Geographic Region: Indian Ocean.

Received 28 May 2003; **Revised** 13 February 2004; **Accepted** 24 March 2004; **Published** 14 May 2004.

Sauter, D., H. Carton, V. Mendel, M. Munschy, C. Rommevaux-Jestin, J.-J. Schott, and H. Whitechurch (2004), Ridge segmentation and the magnetic structure of the Southwest Indian Ridge (at 50°30′E, 55°30′E and 66°20′E): Implications for magmatic processes at ultraslow-spreading centers, *Geochem. Geophys. Geosyst.*, *5*, Q05K08, doi:10.1029/2003GC000581.

Theme: Accretionary Processes Along the Ultra-slow Spreading Southwest Indian Ridge
Guest Editors: Catherine Mevel and Daniel Sauter

1. Introduction

[2] Magnetic studies of mid-oceanic ridges have defined a moderately systematic pattern of the along-axis crustal magnetization variability. High axial magnetic anomaly amplitudes and rock magnetization intensities are observed on tips of ridge segments along the fast-spreading East Pacific Rise (EPR) [e.g., *Sempéré*, 1991]. These high magnetizations are generally associated with Fe-Ti rich basalts resulting from magmatic fractionation in shallow level reservoirs. Along the slow-spreading Mid-Atlantic Ridge (MAR) the amplitude of the axial magnetic anomaly and equivalent magnetization increase also at segment ends at various locations [e.g., *Ravilly et al.*, 1998]. The correlation between iron oxide content and magnetic anomaly amplitudes [e.g., *Weiland et al.*, 1996] suggests that the high magnetic anomaly amplitudes at segment ends of the southern MAR also result from the presence of Fe-Ti rich basalts. However, as magma chambers, if any, are transient features at slow-spreading ridges [*Cannat*, 1996], other explanations such as the presence of serpentinized bodies in the vicinity of discontinuities [e.g., *Pockalny et al.*, 1995; *Ravilly et al.*, 1998], the thickness variation of the magnetic source layer [e.g., *Grindlay et al.*, 1992], the decrease of magnetization at the segment center related to more pervasive faulting and/or the hydrothermal activity [*Tivey and Johnson*, 1987] have also been proposed to account for the observed increase of magnetic anomaly amplitude at segment ends. However, new investigations of the Southwest Indian Ridge (SWIR) and Arctic ridges have revealed that, in contrast with faster-spreading ridges, ultraslow-spreading ridges display small axial discontinuities as well as long amagmatic sections which are marked by weak magnetization relative to the segment centers [*Sauter et al.*, 2001; *Dick et al.*, 2003; *Hosford et al.*, 2003].

[3] In this paper, we investigate the relationships between the segmentation and the magnetic structure of the ultraslow-spreading SWIR. We use off-axis data collected in three survey "boxes" located in domains with contrasted segmentation and mean depth (Figure 1). Survey box A (54°40′–56°40′E) is located in the deep and oblique domain between Gallieni TF (52°20′E) and Melville TF (60°45′E) while survey box B (49°15′–51°20′E) sits in the shallow and slightly oblique domain west of Gallieni TF and survey box C (65°45′–66°45′E) is located in the deepest domain

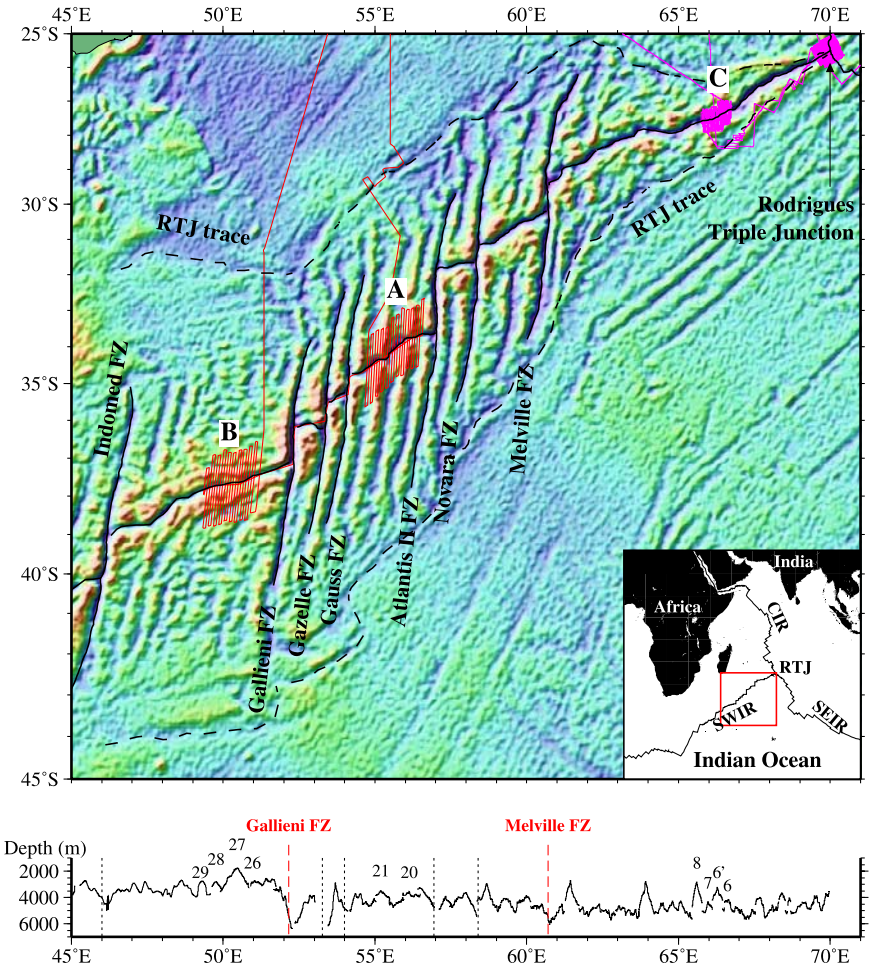

Figure 1. (top) Structural map and (bottom) along-axis bathymetric profile of the Southwest Indian Ridge (SWIR) between 45°E and 71°E. On the structural map, thick black lines indicate the fractures zones, the triple junction traces and the SWIR axis which are interpreted from the free air gravity anomalies (shown in background) derived from satellite sea-surface altimeter measurements [*Smith and Sandwell*, 1995]. Tracks of the Rodriguez cruises are shown by magenta lines. Tracks of the Gallieni cruise are shown by red lines. A, B and C indicate the three survey boxes discussed in the text. SEIR, Southeast Indian Ridge; CIR, Central Indian Ridge; RTJ, Rodrigues Triple Junction. On the bathymetric profile, the segments cited in the text are identified by their number, following the nomenclature of *Cannat et al.* [1999]. Along-axis bathymetric data were collected during the Capsing cruise (R/V L'Atalante, 1993; 57–70°E) [*Patriat et al.*, 1997], the Gallieni cruise (49–57°E) and the SWIFT cruise (R/V Marion Dufresne, 2001; 32–49°E) [*Humler et al.*, 2001]. The Gallieni and Melville FZs bound three major SWIR sections (see text for further details).

of the SWIR to the east of Melville TF. We first show data from survey box A because this area displays two large nontransform discontinuities (NTDs) which have no described equivalent along faster-spreading ridges. We present magnetization maps calculated over at least two ridge segments and two NTDs up to anomaly 5 (~10 Ma) in survey boxes A and B and up to anomaly A3 (~4.5 Ma) in survey box C. The most striking feature of our magnetization solutions is an along-axis decrease of the magnetization for almost all the segments toward the NTDs which is the opposite to what is typically described at faster-spreading ridge axes. However, this along-axis magnetization decrease disappears off-axis and magnetizations observed along the traces of NTDs are higher than in the segments. Moreover, the magnetic reversal pattern is no more observed along some NTD traces. We discuss the processes that may control this magnetic structure of the

SWIR and the implications for magmatic processes at ultraslow spreading centers.

2. Regional Setting

[4] The SWIR is a major plate boundary separating Africa and Antarctica with an ultraslow spreading rate of about 16 km/m.y. [*Patriat and Ségoufin*, 1988]. The mean axial depth, the obliquity of the ridge axis (with respect to the normal to the spreading direction: N0°E at 60°E; [*Patriat and Ségoufin*, 1988; *Chu and Gordon*, 1999]), the segmentation style and the presence or absence of long-lived axial discontinuities vary along axis between Indomed TF (46°E) and the Rodrigues triple junction (RTJ, 70°E) whereas the spreading rate is almost constant. These variations allow defining three main ridge sections bounded by two major transform faults, the Gallieni and Melville TFs [*Cannat et al.*, 1999; *Sauter et al.*, 2001]. The mean axial depth increases eastward from 3090 m to 4330 m across Gallieni TF system and from 4330 m to 4730 across Melville TF (Figure 1). This large-scale variation of axial depths suggests that the regional density structure of the axial region also varies from a thinner crust and/or colder mantle beneath the deepest ridge section, between 61°E and 69°E, to a thicker crust and/or hotter mantle beneath the shallow ridge section to the west of Gallieni TF. Differences in mantle temperature and in melt thickness between these two regions have been estimated to ~100°C and ~4 km respectively, using a simple model of mantle melting and regional isostatic compensation [*Cannat et al.*, 1999]. The along-axis variation of geochemical characteristics also shows that the basalts with the highest degree of partial melting along the SWIR are found to the west of Gallieni TF [*Meyzen et al.*, 2003] while very low-degree of melting of abyssal peridotites are estimated in the eastern section of the SWIR [*Seyler et al.*, 2003]. The sections to the west of Gallieni TF and to the east of Melville TF are slightly oblique (with a 20° and 25° overall obliquity, respectively) while the axial domain in the ridge section between these two transform faults is strongly oblique (45° overall obliquity). This oblique section of the SWIR is characterized by many long-lived axial discontinuities whereas the two less oblique sections are devoid of such long-lived discontinuity (Figure 1).

3. Data Collection and Processing

[5] During the Gallieni cruise of the R/V L'Atalante in 1995 over survey boxes A and B, navigation was obtained using the Global Positioning System (GPS). During the Rodriguez cruises of the R/V Jean Charcot in 1984 over survey box C, navigation was based on Transit satellite system. Final navigation of the Rodriguez cruises was obtained by minimizing crossover errors in the high resolution Seabeam bathymetry [*Munschy and Schlich*, 1990].

3.1. Processing of Magnetic Data

[6] Total magnetic field data were collected using towed proton precession magnetometers along approximately north-south flow line parallel profiles. These data were corrected for the regional magnetic field using the definitive geomagnetic reference field (IGRF 9th generation) for 1984 and for 1995 [*Macmillan et al.*, 2003]. Recordings of the magnetic field at Martin de Viviès observatory (New-Amsterdam island), Port-Alfred observatory (Crozet island) and Hermanus observatory (South Africa) showed that several geomagnetic storms occurred during the surveys producing irregular variations and resulting in large crossover errors up to 70 nT. We have removed such variations of the external magnetic field using these observatory recordings and the crossover analysis of magnetic anomaly profiles (see Appendix A). The mean of the absolute value of the magnetic anomaly differences at crossover points decreases significantly from 12.8 to 6.7 nT in survey box A, from 23 to 17.6 nT in survey box B and from 12.7 to 7.6 nT in survey box C. We have interpolated magnetic anomaly values between the ship tracks using a minimum curvature algorithm [*Smith and Wessel*, 1990] on an anisotropic grid. Since the magnetic data are averaged over 1 min, we have data every ~300 m (at 10 knots) along the ship tracks that are spaced every ~3 km in survey box C and every ~7 km in survey boxes A and B. Following *Weiland et al.* [1996], we have created magnetic anomaly grids with many nodes along-track (every 0.5 nautical miles) and

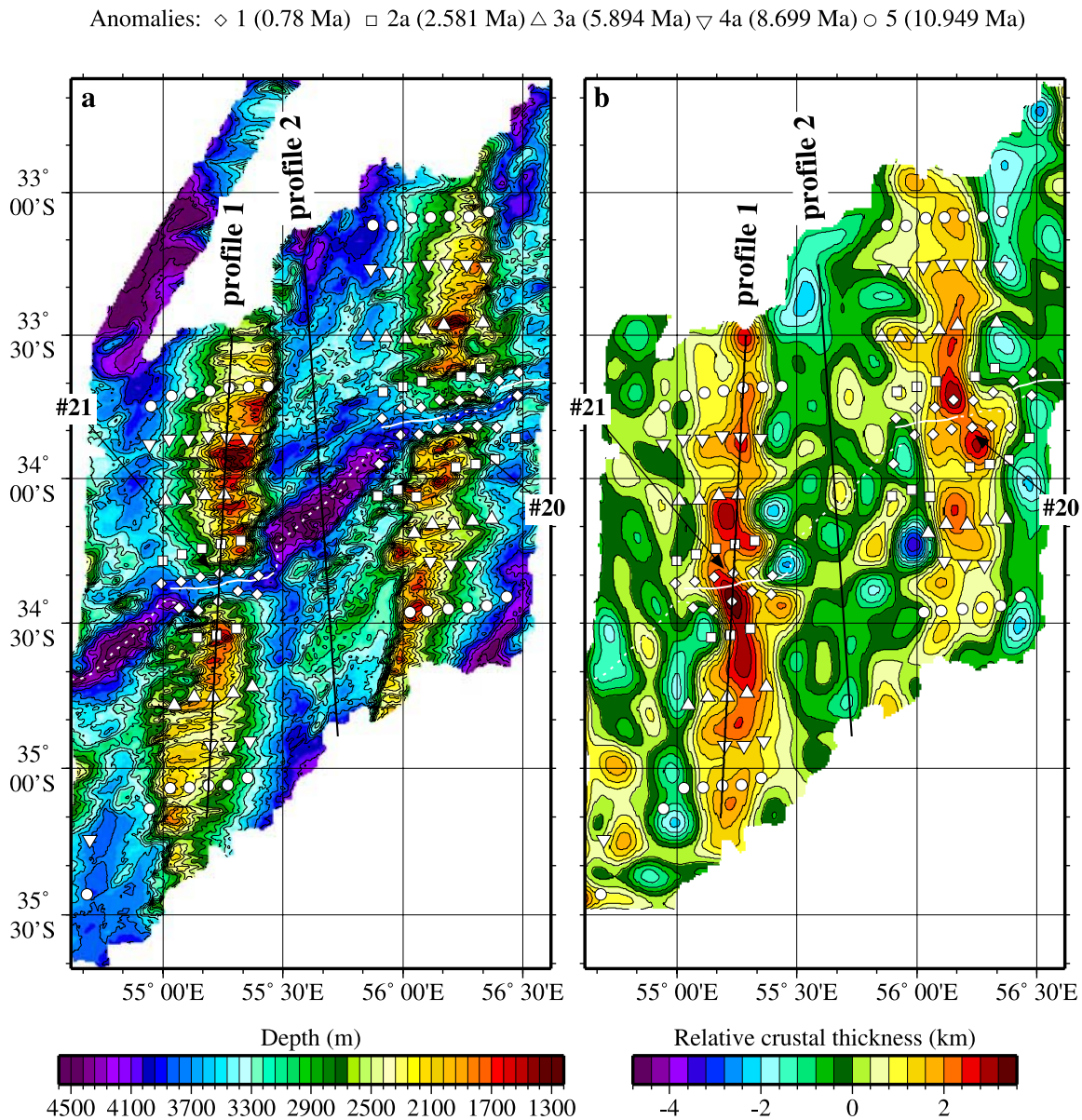

Figure 2. (a) Bathymetric map, (b) crustal thickness variation map, (c) magnetic anomaly map, and (d) magnetization distribution of survey box A along the SWIR between 54°27′E and 56°37′E. Color interval and contour interval of the bathymetric map are every 80 m and every 160 m, respectively. Color and contour intervals of the crustal thickness variation map are every 400 m. The color and contour intervals of the magnetic anomaly map is every 100 nT. The color and contour intervals of the magnetization map is every 2 A/m. The magnetization distribution is calculated by a three-dimensional inversion of the magnetic anomaly map in the presence of bathymetry (see text for further details). Thick white lines indicate the axis: continuous along the neovolcanic axis in the segments and dotted along the deepest points of the NTDs. Segments indicated by #20 and #21 are restricted to the portions of the axis which trend almost perpendicular to plate motion. The symbols indicate the magnetic anomaly picks on two-dimensional magnetic profiles [*Mendel et al.*, 2003].

fewer across-track (every 2 nautical miles) mimicking the data distribution. For the inversion, these grids are then sampled at 1 nautical mile (Figures 2c, 3c, and 4c). This technique attempts to minimize the loss of the shorter wavelength signals and better retain amplitude information needed to understand crustal magnetization patterns.

[7] A three-dimensional inversion for crustal magnetization was performed to account for the dis-

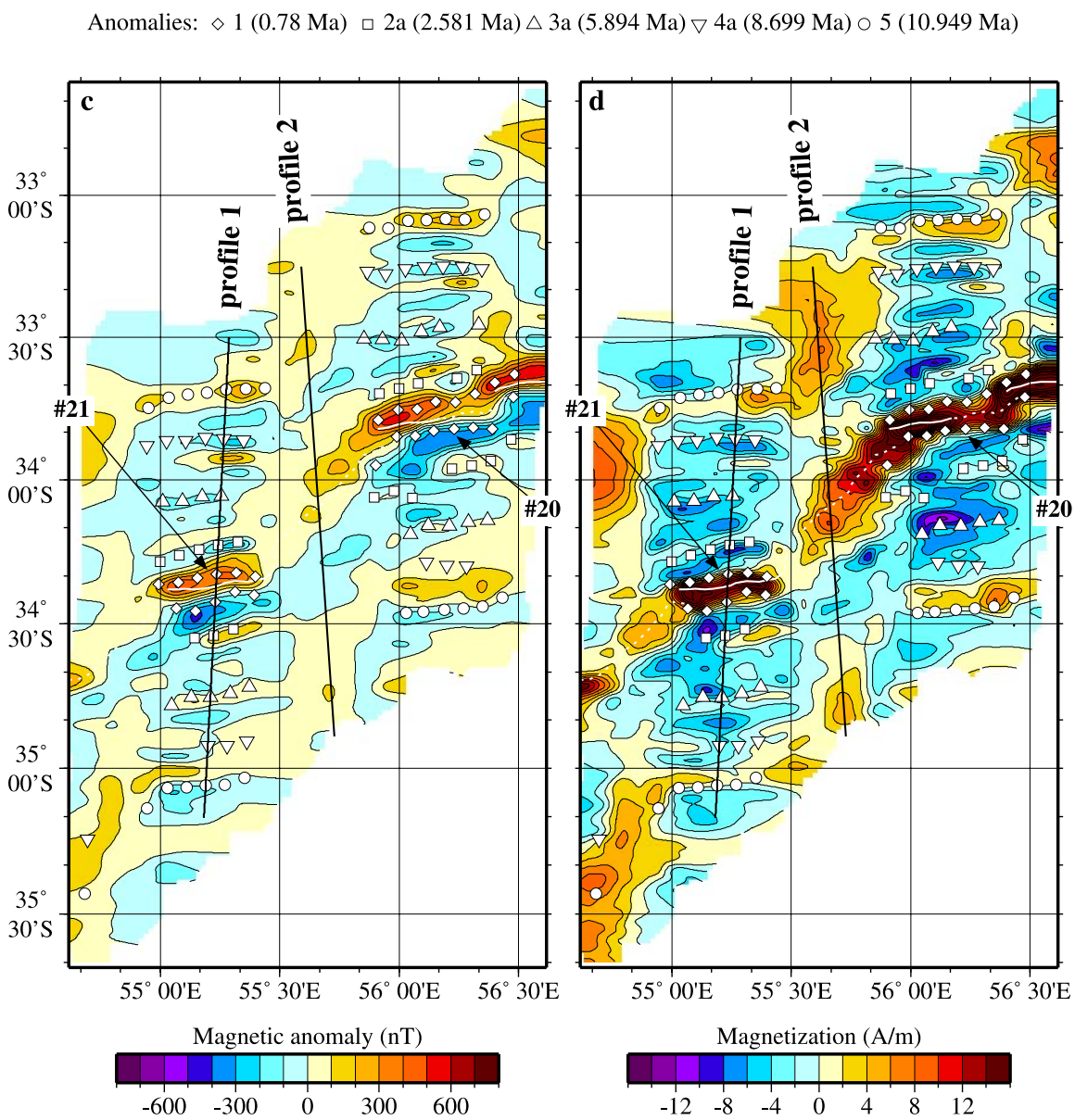

Figure 2. (continued)

torting effects of seafloor topography and skewness. We used the Fourier technique of *Parker and Huestis* [1974] and extended for grid analysis by *Macdonald et al.* [1980] which assumes a source layer of constant thickness (0.5 km) and an upper boundary defined by the bathymetry. The inversion emphasizes the lateral variations in crustal magnetization but cannot distinguish changes in source thickness or source intensity. We assumed a direction of magnetization that corresponds to a geocentric axial dipole and mirror both the bathymetric and magnetic input grids to minimize the edge effects of the Fourier transform. To ensure convergence during the inversion, we employed cosine tapered band-pass filters with long- and short-wavelength cutoffs of 400 and 3.5 km. As the magnetization solutions are more or less balanced over the Brunhes/Matuyama reversal, no annihilator has been added to these solutions which are shown in Figures 2d, 3d, and 4d.

[8] The magnetization solution of survey box B shows a shift toward more positive magnetization

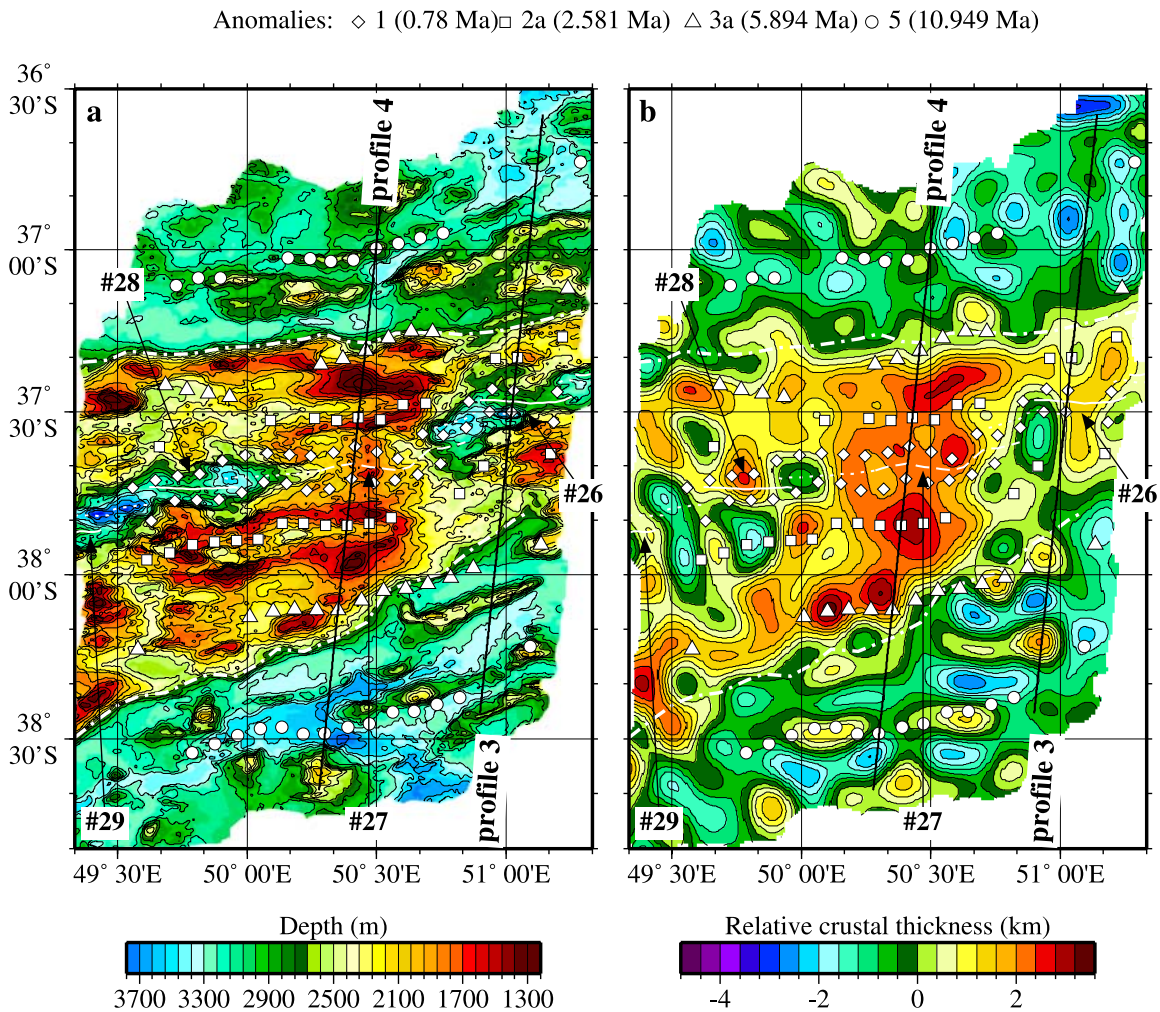

Figure 3. (a) Bathymetric map, (b) crustal thickness variation map, (c) magnetic anomaly map, and (d) magnetization distribution of survey box B along the SWIR between 49°20′E and 51°20′E. Same caption as in Figure 2. Thick dashed and dotted lines indicate the edges of the central shallow and thick crust area.

values toward the distal part of the flanks. As such a long wavelength signal in the result of the inversion is always suspect, we have also calculated the crustal equivalent magnetization using a generalized inversion method [e.g., *Sichler and Hékinian*, 2002] which generates no spurious long wavelength component. This method is based on a linear discrete inversion taking as unknowns the magnetization of parallelepiped shaped prisms which fit the topography. As the obtained magnetization solutions are almost identical (difference <2 A/m) we conclude that the observed more positive magnetization values toward the distal part of survey box B are meaningful.

[9] Finally, two-dimensional forward modeling has been used to identify the magnetic anomalies. A model profile using the geomagnetic reversal timescale of *Cande and Kent* [1995] is shown for comparison with a profile of survey box A in Figure 5. We assume a constant 500 m thick magnetic layer draped on the bathymetry with a 20 A/m magnetization for the Brunhes period and a uniform ±4 A/m magnetization off-axis. The effect of sloped polarity boundaries on magnetic anomaly amplitude has been ignored in the modeling. A good fit was achieved by choosing 12–16 km/m.y. spreading rates during asymmetric crustal accretion (5–25% asymmetry in spreading half rates). Spreading rates and magnitudes of spreading asymmetry are given in

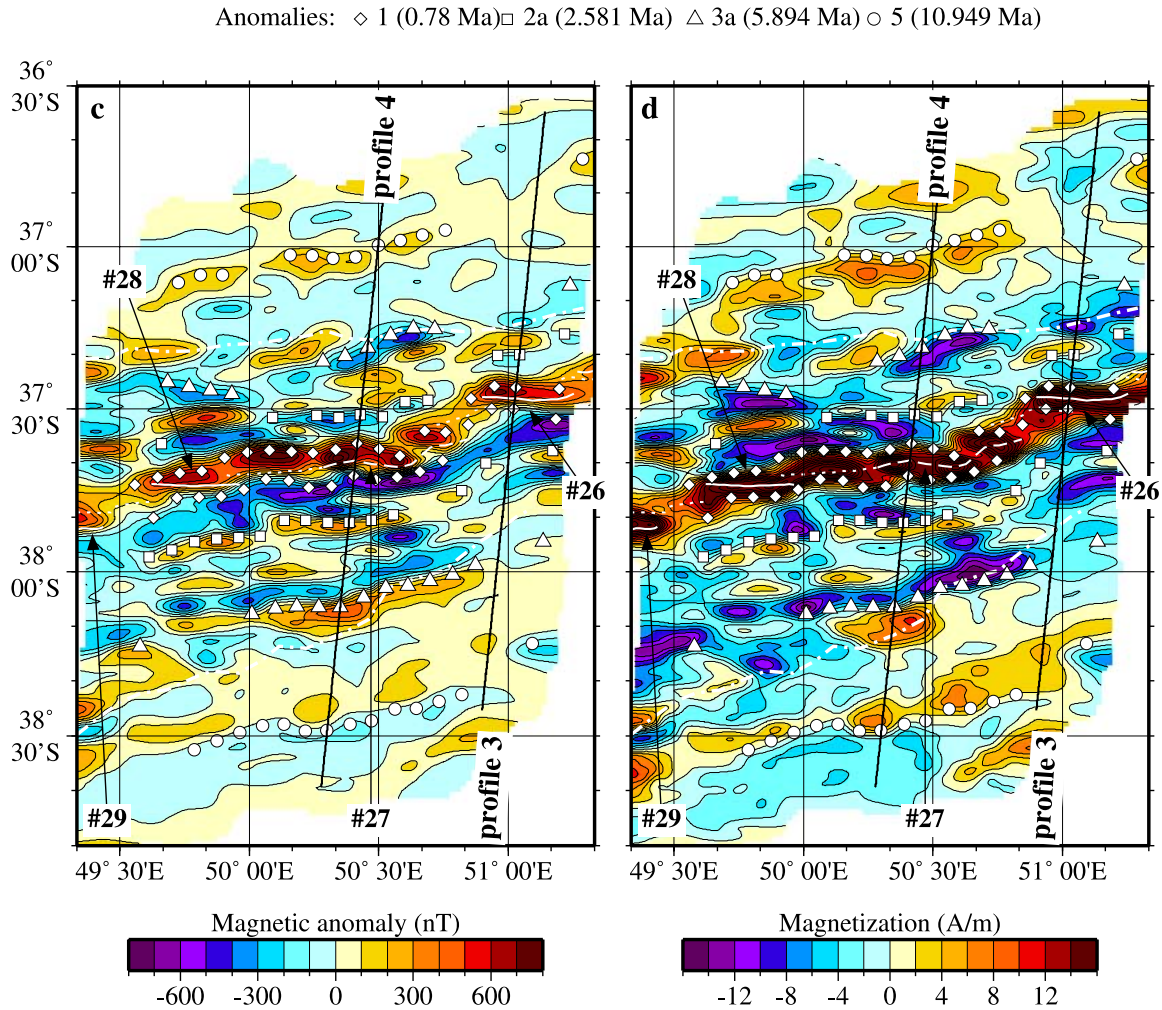

Figure 3. (continued)

Mendel et al. [2003] for survey boxes A and B; and in *Cannat et al.* [2003] for survey box C.

3.2. Processing of Gravimetry Data

[10] The crustal thickness variation maps shown in Figures 2b, 3b, and 4b were deduced from residual gravity anomaly following *Rommevaux et al.* [1994]. The effect of a constant thickness, constant density (2700 kg/m^3) crust was removed from free air anomaly data to obtain Mantle Bouguer Anomaly (MBA) values. We have calculated the effect of cooling of the plates with age as a function of distance to the ridge axis, using the poles and rates of plate motion of [*Patriat and Ségoufin*, 1988]. The gravity effect of cooling of the plates with age was removed from the MBA. We then inverted these residual anomalies for crustal thickness following the method of *Kuo and Forsyth* [1988]. This method assumes that gravity anomalies only reflect crustal thickness variations. A crustal thickness of 3 km has been chosen to calculate the MBA map of survey box C so that the gravity derived crustal thickness estimates were similar to seismic crustal thickness values along the 100 km-long CAM116 profile [*Muller et al.*, 1999] (see *Cannat et al.* [2003] for a detailed comparison). As survey boxes A and B are located in shallower sections of the SWIR with inferred thicker crust [*Cannat et al.*, 1999] we chose a 5 km crustal thickness to calculate the MBA maps.

4. Ridge Segmentation in the Three Survey Boxes

[11] The criteria used to define any ridge segmentation pattern are mainly the along-axis variations

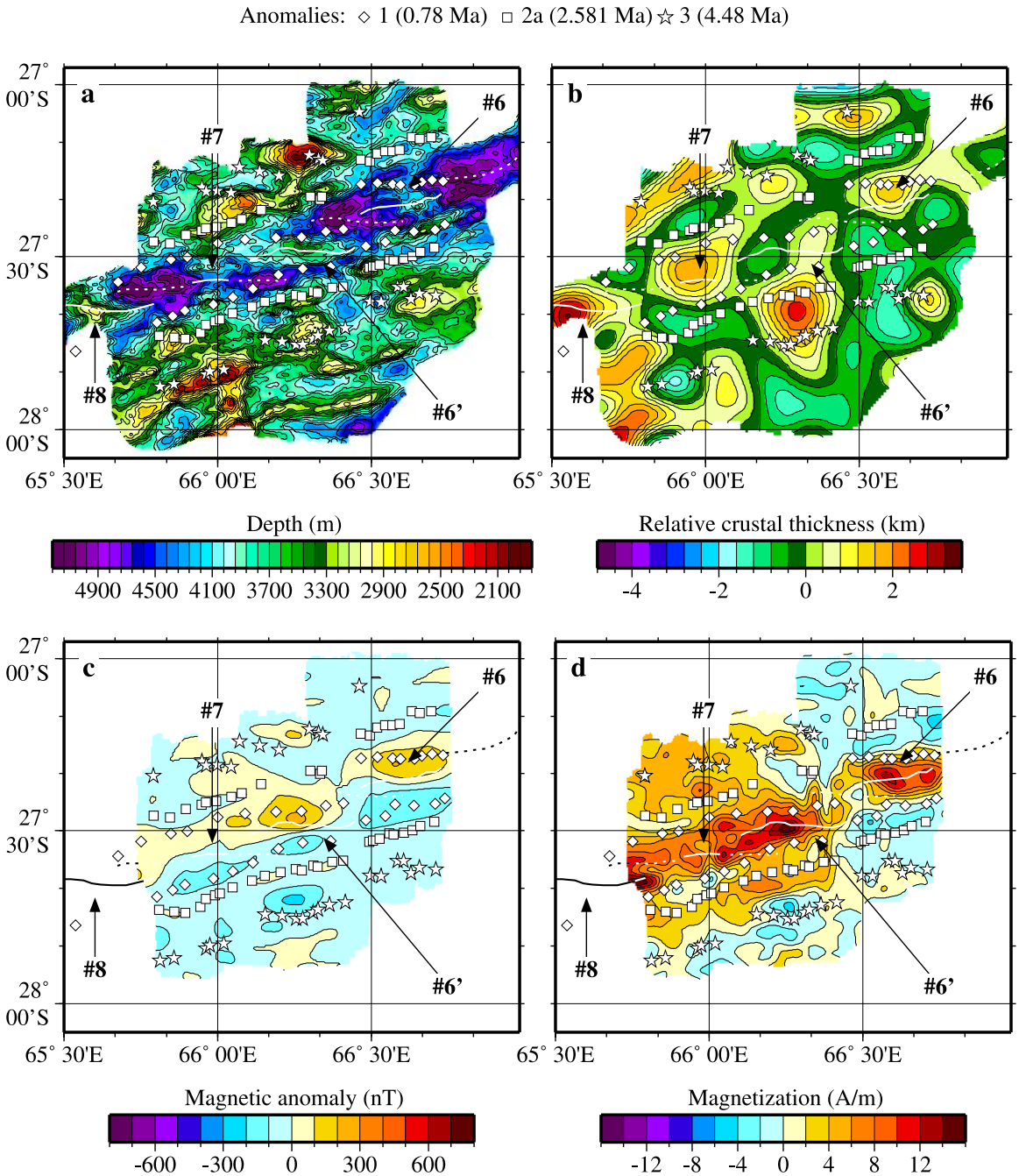

Figure 4. (a) Bathymetric map, (b) crustal thickness variation map, (c) magnetic anomaly map, and (d) magnetization distribution of survey box C along the SWIR between 65°30′E and 67°E. Same caption as in Figure 2 except that magnetic anomaly picks are from *Cannat et al.* [2003].

of the valley floor depth, together with offsets of the axis occurring at segment ends. Because axial discontinuities are much larger at the SWIR than on the MAR [e.g., *Rommevaux-Jestin et al.*, 1997], we have chosen to restrict the segments to the portions of the axis which trend almost perpendicular to plate motion and identify the NTDs as the strongly oblique and deeper portions of the axis which offset these segments.

4.1. Survey Box A

[12] The along-axis depth profile between Gallieni and Melville TFs looks like that of slow spreading

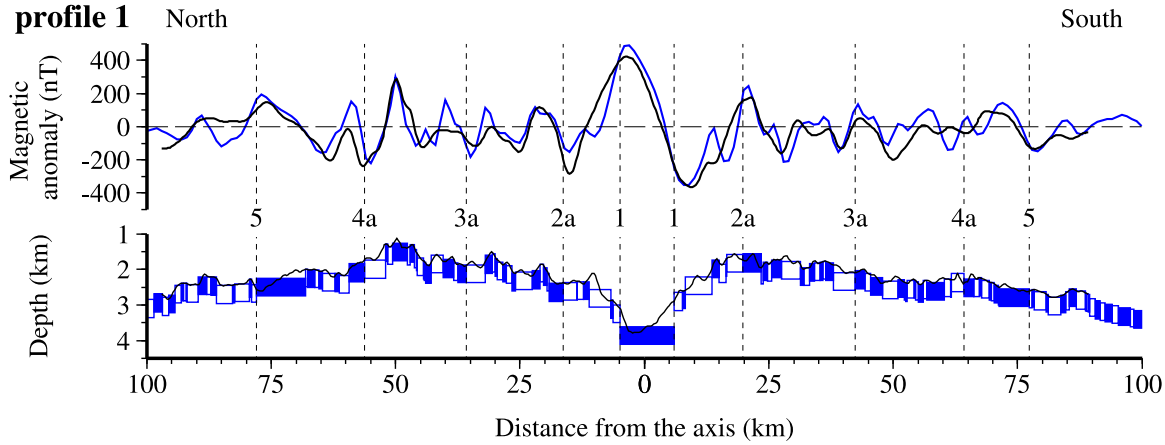

Figure 5. Magnetic anomaly identification along magnetic anomaly profile 1 over segment # 21 (black line; see location of profile 1 in Figure 2). The synthetic magnetic anomaly profile (in blue) is calculated from a two-dimensional block model incorporating the calibrated magnetic inversion timescale of *Cande and Kent* [1995], with 12–16 km/m.y. spreading rates during asymmetric crustal accretion (5–25% asymmetry in spreading half rates; see *Mendel et al.* [2003]). We assume a constant 500 m thick magnetic layer draped on the bathymetry with a 20 A/m magnetization for the Brunhes period and a uniform ±4 A/m magnetization off-axis. The effect of sloped polarity boundaries on magnetic anomaly amplitude has been ignored in the modeling.

ridges with relatively homogeneous segment lengths and reliefs (Figure 1). The segmentation in survey box A consists of 40–45 km long segments centered at 56°08′E and 55°12′E, respectively (segments #20 and #21 in the nomenclature of *Cannat et al.* [1999]). These two segments correspond to high reliefs (ΔR = 900–1300 m high measured along-axis) with a narrow axial valley (10–15 km wide) (Figure 2a) [*Sauter et al.*, 2001]. Segment #21 is bounded by two N40–50°E trending, deep and wide NTDs (20–30 km wide) which offset the axis by 40 and 65 km (Figure 2a). Segments #20–21 have a 2–3 km on average thicker crust than the large NTDs, on the axis as well as on the flanks (Figure 2b) [*Mendel et al.*, 2003]. There is a small 150 m-high axial volcanic ridge (AVR) on top of segment #21 while there is no AVR in segment #20 although a few volcanoes are observed in its shallowest part. To the east of segment #20 the axis is indicated by a prominent EW-trending AVR within an axial valley that widens and deepens toward Atlantis II TF [*Dick et al.*, 1991]. A small N55°E trending basin offsets this last ridge section and segment #20 by about 11 km (Figure 2a). The off-axis traces of segments #20–21 are easy to follow off-axis and correspond to large bathymetric highs parallel to the spreading direction. Superimposed on these bathymetric highs, abyssal hills form elongated ridges, perpendicular to the spreading direction (Figure 2a). These bathymetric highs are bordered by relative depressions corresponding to the NTDs off-axis traces [*Mendel et al.*, 2003].

4.2. Survey Box B

[13] The present-day segmentation in survey box B consists of four segments (#26–28 and the eastern end of segment #29) limited by four NTDs [*Sauter et al.*, 2001]. A striking feature of this survey area is the 85-km-long very high relief (ΔR = 1900 m) segment #27 centered at 50°28′E (Figure 3a). The axial valley disappears in the shallowest section (<1600 m) of this segment where numerous flat-topped volcanoes are observed but no AVR. To the west and to the east of this segment, NTDs offset the axis by 10 km and 18 km, respectively, and bound 40 km-long smaller segments (ΔR = 650 m) crowned by EW-striking volcanic ridges. Segments have a 2–3 km on average thicker crust than the large NTDs (Figure 3b) [*Mendel et al.*, 2003]. The most striking features on the flanks are two large outward facing scarps, located at 40–70 km from the axis, which bound a central axial domain 1000–1500 m shallower than the older lithosphere (Figure 3a). This shallow axial domain corresponds

to an area of 2–3 km thicker crust (Figure 3b). Its V-shape, pointing toward the east, observed both in the bathymetric and crustal thickness maps, suggests the propagation of a melting anomaly. The off-axis trace of the segmentation is less well marked than in survey box A. Segment #27 and the largest NTDs between segments #27–26 and #28–29 can hardly be trace back until the edges of the shallow axial domain (Figures 3a–3b). Moreover, the off-axis trace of the small NTD between segment #27 and #28 cannot be identified. The segmentation is highly unstable in the deeper area further onto the flanks where bathymetric highs are randomly distributed and most of them are underlain by thin crust.

4.3. Survey Box C

[14] The ridge section east of Melville TF is characterized by very high relief segments (ΔR up to 2600 m) thought to be large volcanic constructions spaced every ~200 km [*Cannat et al.*, 1999]. Survey box C is located between such high relief segments. The segmentation consists in two segments (#6–7 at 66°37′E and 65°59′E; Figure 4) with weak along-axis reliefs (ΔR < 1200 m) and crustal thickness variations (2 km on average). Seismic refraction results show a 6 km thick crust beneath the high relief segment #8 to the west of the survey area while the crust is only 3.5 km thick beneath segment #7 and 2.0–2.5 km thick in the adjacent NTDs [*Muller et al.*, 1999]. This crustal thickness variation results from large changes in oceanic layer 3 thickness (0–3.5 km) while the thickness of layer 2 is relatively constant (~2 km) [*Muller et al.*, 1999]. The bathymetric swell located at 66°16′E (#6′ in Figure 4) displays a large along-axis relief (ΔR = 1800 m; [*Mendel et al.*, 1997]) but corresponds to a thin crust area (Figure 4b) [*Rommevaux-Jestin et al.*, 1997]. It is therefore clearly an uncompensated feature and has not been identified as a segment by *Cannat et al.* [1999]. This prominent ridge does, however, bear a large amplitude central magnetic anomaly [*Patriat et al.*, 1997] and was therefore interpreted as an AVR [*Mendel et al.*, 1997]. Segment #6 also displays a small AVR while there is no volcanic ridge in segment #7. The offsets of the axis are small in this survey area (<19 km) which presents no clear off-axis organization suggesting that the axial segmentation is short-lived.

5. Magnetization Results

[15] The variability in crustal magnetization was examined both off-axis and along the neovolcanic axis in the segments and along the deepest point of the axial valley in the NTDs. We have defined the neovolcanic axis as the crest of the AVR and the alignment of volcanoes in the absence of an intra-rift ridge in the segment.

5.1. Survey Box A

[16] The neovolcanic axis in segments #20–21 is characterized by 15–25 A/m higher magnetization values than the axis in the largest NTDs (Figures 2d and 6). The decrease of the magnetization from the segments ends toward the large NTDs mimics the along-axis bathymetric slope and is sharp to the east of segment #21 whereas it is gentle westward of segments #20 and #21. As segments #20–21 have thicker crust than the large NTDs, high magnetization values also correlate with thick crust areas at the segment scale. However, the fine scale (<20 km) crustal thickness variations do not correlate with the along-axis magnetization variations (Figure 6). Between segment #20 and Atlantis II TF, the crust thins strongly eastward while high magnetization values are observed along a prominent AVR. The small offset between segment #20 and this AVR has magnetization values only 10 A/m smaller than along the neovolcanic axis. There is also a small low magnetization anomaly at the center of segment #21 (<5 A/m variation).

[17] The magnetic reversal pattern is only observed in the off-axis traces of segments #20–21 while no lineation is observed along the off-axis traces of the NTDs (Figure 2d). There is a sharp decay in the values of magnetizations from the neovolcanic axis in segments #20–21 out to older lithosphere. This decay reaches 14–23 A/m from the axis to A5. However, the real long-term decay in segments #20–21 cannot be resolved accurately with our data because of the lack of resolution in sea surface data due to the filtering effect of water depth and the short reversal spacing for slow spreading rates

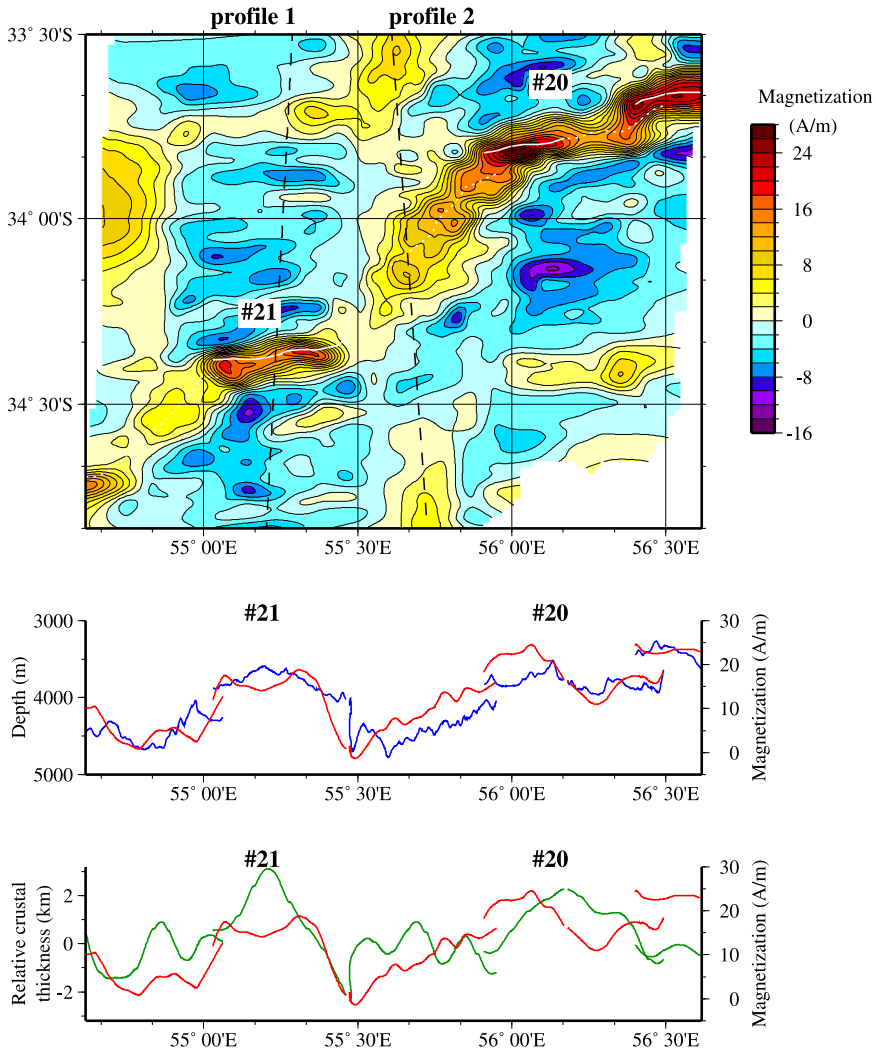

Figure 6. Along-axis magnetization distribution in survey box A. The color and contour intervals of the magnetization map is every 2 A/m. The along-axis variation of the magnetization distribution (red line) is compared to the along-axis depth profile (blue line) and to the along-axis crustal thickness variations (green line).

[*Tivey and Tucholke*, 1998]. Such marked near axis decay in magnetization has been observed on the EPR and MAR [e.g., *Pariso et al.*, 1996] and it is attributed to progressive low-temperature oxidation of the extrusive basalt layer [e.g., *Macdonald*, 1977]. This long-term variation is significantly different in the NTDs as magnetization is lower at the axis in those areas and as it increases toward the flanks of the large NTDs. This increase of the magnetization starts at 10–30 km from the axis and reach magnetization values 2–4 A/m higher in the large NTDs than in the segments at A5 time (Figure 7). This rise to more positive magnetization with age in both flanks of the large NTDs regardless of polarity and the lack of magnetic reversal pattern in those areas thus strongly suggest that the original remanent magnetization strongly decreases and is replaced with induced magnetization. However, the northernmost part of these NTDs displays a decrease of the magnetization after A5 time suggesting that remanent magnetization may not be completely destroyed. As edge effects cannot be excluded during the inversion, longer profiles along the NTD traces are needed to constrain the variation of remanent magnetization after A5 time.

5.2. Survey Box B

[18] As in survey box A, the magnetization values along the neovolcanic axis of segments #28 and 26

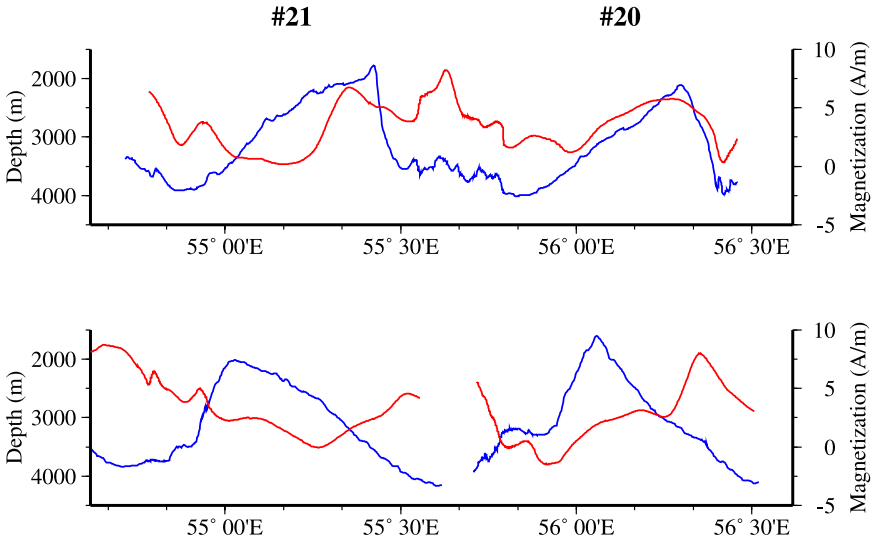

Figure 7. Magnetization variation (red line) and depth profile (blue line) along isochron A5 on the (top) northern flank and (bottom) southern flank of survey box A.

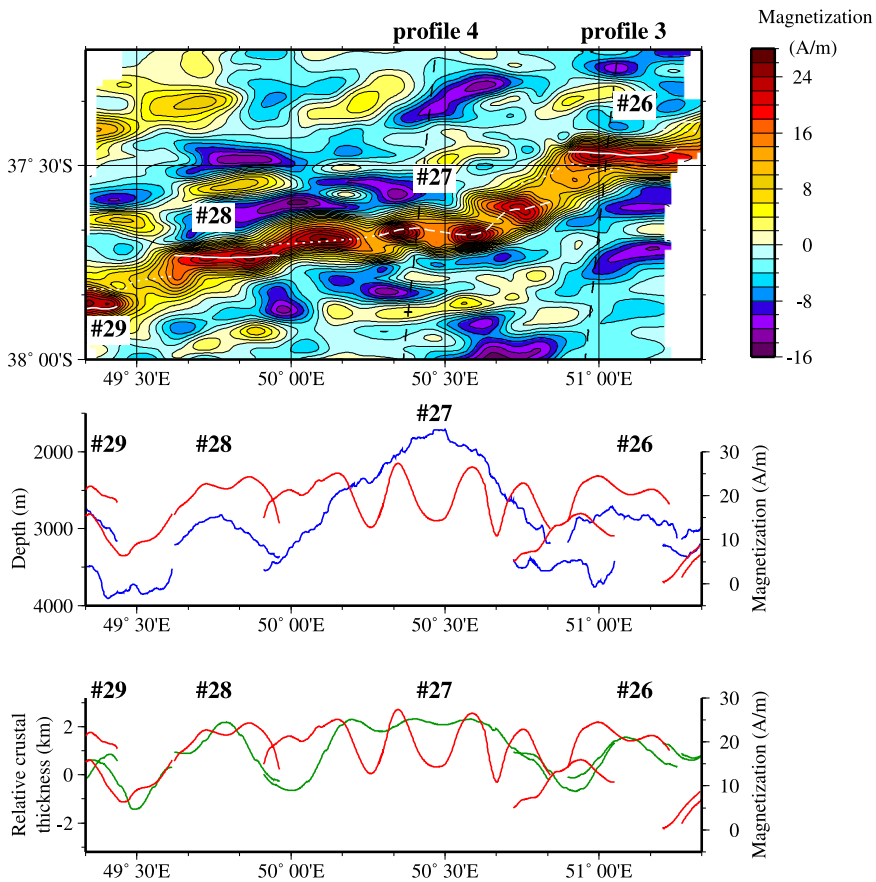

Figure 8. Along-axis magnetization distribution in survey box B. The color and contour intervals of the magnetization map is every 2 A/m. The along-axis variation of the magnetization distribution (red line) is compared to the along-axis depth profile (blue line) and to the along-axis crustal thickness variations (green line).

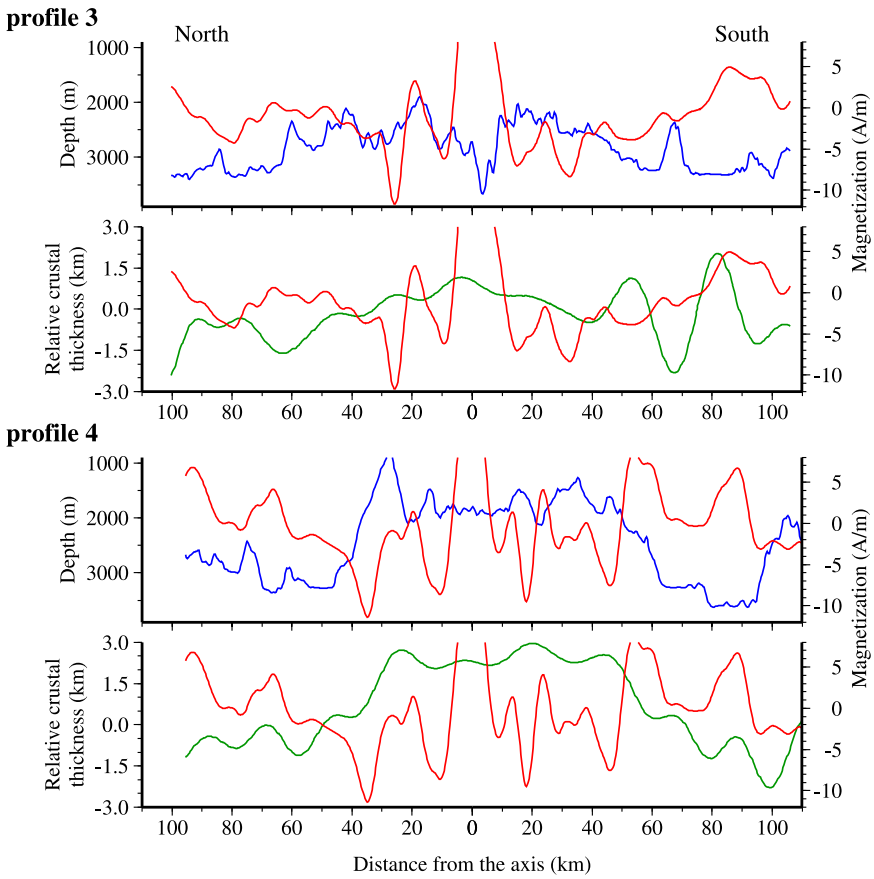

Figure 9. Magnetization variation (red line), depth (blue line) and relative crustal thickness profiles (green line) for profile 3 and 4 in segments #26–27 in survey box B. Note the shift toward more positive magnetization values outside the thicker crust and shallower axial domain.

are up to 18 A/m higher than in the adjacent NTDs (Figures 3d and 8). Crustal thickness variation between segments of this survey area falls also in the same range (2.5–3 km) than in survey box A. The center of segment #27 displays 10 A/m lower magnetization values than the ends of this segment (Figure 8). Moreover, magnetization values as high as along the AVRs of segments #28 and #26 are also observed in the adjacent NTD between segments #27–28 and the western part of the NTD between segments #27–26. As in segment #21 in survey box A, there is also a weak magnetization low at the center of segment #28 (<5 A/m variation). Such magnetization variation along segment #27, and in a much lesser extent along segment #28, looks thus similar to the along-axis variations at the MAR where magnetization is found to be weakest at segment centers and higher at segment ends [e.g., *Pariso et al.*, 1996].

[19] The most striking feature of our magnetization solution on the flanks of survey box B is the increase of the magnetization outside the shallow and thick axial domain (Figure 3d). Overall more positive magnetization values are observed in the deeper, older and thinner crust areas in all parts of survey box B, regardless of polarity (Figure 9). This shift toward more positive magnetization values suggests the presence of an induced component of magnetization in the thin crust areas. The outward facing scarps which bound the shallow axial domain are oblique to the magnetic reversal pattern and draw a V pointing eastward indicating that the thickening of the crust has propagated eastward (Figure 3d). Spreading has been asymmetric during the last 11Ma leading to a wider shallow axial domain on the southern flank (Figures 5 and 9). Asymmetric spreading resulting in wider intervals of constant polarity on the

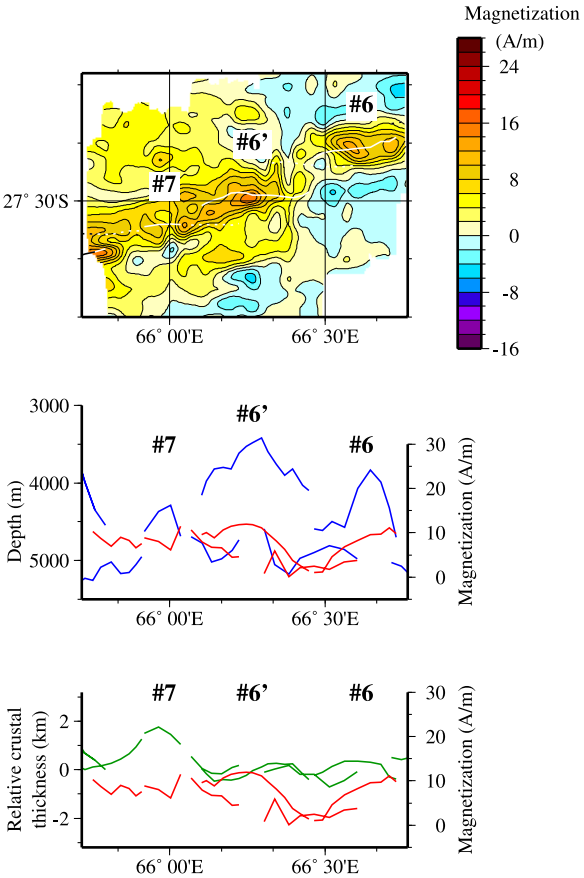

Figure 10. Along-axis magnetization distribution in survey box C. The color and contour intervals of the magnetization map is every 2 A/m. The along-axis variation of the magnetization distribution (red line) is compared to the along-axis depth profile (blue line) and to the along-axis crustal thickness variations (green line).

southern flank of segment #27 may also explains the clearer lineations with higher magnetization values observed on this flank. In contrast with survey box A the magnetic reversal pattern in this survey area can be observed in both the traces of the NTDs and of the segments. However, slightly more positive magnetization values are found along the NTDs traces in the shallow axial domain. In the deeper areas further onto the flanks, the highly unstable segmentation results in no noticeable systematic magnetization variations (Figure 3).

5.3. Survey Box C

[20] The amplitude of the magnetization variations along the axis in survey box C (10 A/m) is twice as small as in survey boxes A and B (Figure 10). The magnetization values are 10 A/m higher along the neovolcanic axis of segment #6 than in the adjacent NTD (Figure 10). The highest magnetization values are found along the AVR centered at 66°16′E and corresponding to a thin crust area (#6′ in Figure 4). Only small magnetization variations (<3 A/m) around a mean value of ~7 A/m are observed along segment #7 and the adjacent NTDs (Figure 10) where seismic data show a relatively constant oceanic layer 2 [*Muller et al.*, 1999]. The segmentation is short-lived in this survey area and no clear off-axis organization is noticable in our magnetization solution (Figure 4).

6. Discussion

6.1. Axial Magnetization Controlled by the Extrusive Lavas

[21] For all segments of the three survey areas, except for segments #27 and #7, magnetization diminishes from high values along the AVRs and alignments of volcanoes to low values in the NTDs where AVRs are no more observed. Because most of the segments correspond to thick crust areas, magnetization variations also correlate with crustal thickness variations at a large scale. However, the along-axis magnetization variations are found independently of smaller-scale crustal thickness variations. Small thin crust areas (<~25 km long) may indeed display high magnetization values along an AVR (as in segment #20). Seismic results from segment #7 in survey box C show strong thickness variations of layer 3 [*Muller et al.*, 1999] while the magnetization values do not display significant changes and rather correlate with the relatively constant thickness of layer 2 in this survey area. Moreover, samples of rift valley basalts from segment #7 and adjacent NTDs between 65°40′E and 66°20′E exhibit relatively constant iron and titanium contents [*Robinson et al.*, 1996]. Further, an empirical relationship between FeO content and natural remanent magnetization (NRM) [*Gee and Kent*, 1998] yields predicted NRM values (10 A/m) which are close to the axial magnetization values obtained by magnetic inversion. The extrusive basaltic layer seems thus to be the most dominant

source of the axial magnetization as previously suggested [e.g., *Schouten et al.*, 1999]. This runs counter to a recent suggestion that gabbros were a likely cause of the change in axial magnetization along the SWIR [*Hosford et al.*, 2003]. Assuming that, as in survey box C and along the faster spreading MAR [*Tolstoy et al.*, 1993], crustal thickness variations in survey boxes A and B mostly occur at the expense of seismic layer 3, we speculate that a strong magnetic contribution of the lower crust would result in an along-axis correlation between the small-scale crustal thickness and magnetization variations. On the contrary we rather observe a direct and strong correlation between the deepening of the axial valley inner floor and the decrease of the magnetization from the extremities of the neovolcanic axis toward the deepest parts of the largest NTDs. This decrease is strong where the along-axis bathymetric slope is steep and weak where the slope is gentle. Such a correlation between the deepening of the axis and the magnetization variation may be explained if this variation is mainly related to near surface changes in the shallow part of the crust and not to deep sited variations.

[22] The systematic sampling of the SWIR axial valley between 9°–25°E and 52°–68°E revealed that serpentinized peridotites frequently crop out in the deepest part of the axis suggesting a thin and discontinuous basalt carapace in the amagmatic sections between the segments [*Seyler et al.*, 2003; *Dick et al.*, 2003]. To determine whether thinning of the basaltic source layer is a viable mechanism for the observed variations of the axial magnetization, two-dimensional forward calculations have been performed along 6 across-axis profiles through the NTD between segments #20–21. We used the chemistry of rift valley basalts [*Meyzen et al.*, 2003] and the empirical relationship between FeO content and NRM of *Gee and Kent* [1998] to predict a 20 A/m magnetization for the source layer (for a mean FeO content of 9.86% in survey box A). This axial magnetization agrees remarkably well with magnetization amplitudes obtained by magnetic inversion in segments #20–21 (Figure 6). As NRM intensity of basalts quickly decreases with increasing age [*Zhou et al.*, 2001] we assume a ±4 A/m magnetization for periods older than the Brunhes one. The amplitude of the central magnetic anomaly was well estimated with models using a source layer thickness decreasing from 500 m on top of the segments (Figure 5) up to 100 m in the deepest part of the NTD. Figure 11 shows such a model computed with a 250 m source layer thickness for profile 2 located in the NTD half way between the segments. Our models do not reproduce the larger width of the central magnetic anomaly in the NTD than in the segments. It may result from 3D effects and juxtaposition of blocks of different polarities within the NTD [e.g., *Collette et al.*, 1974] and needs further refinement in the modeling. An alternative explanation for the observed variations of the axial magnetization is a decrease of the intrinsic magnetization of the basalts toward the deepest part of the NTD due to magnetic mineralogy. However, the FeO content of fresh basaltic glasses is variable in the NTD [*Meyzen et al.*, 2003] yielding to 10–30 A/m predicted NRM values. Contributions of such intrinsic variations can thus not be excluded but cannot explain alone the observed decrease of the axial magnetization toward the NTDs.

[23] A thin basaltic carapace in the large NTDs suggests less frequent volcanic eruptions than in the segment centers. About 50% lower seafloor reflectivity in the large NTDs [*Sauter et al.*, 2001] also indicates a thicker sedimentation cover resulting from both the accumulation of sediments in intra-rift basins through the action of bottom currents and from an older volcanic seafloor in these basins with less frequent volcanic eruptions affecting the sediment cover [*Sauter and Mendel*, 1997]. Such variation of the seafloor reflectivity is not observed at smaller NTDs, like the one to the east of segment #20 where the variation of the magnetization is smaller than in the larger NTDs [*Sauter et al.*, 2001]. In survey box C, small magnetization variations are also observed along short-lived segment separated by small offsets with smaller along-axis crustal thickness variations than those at the large NTDs of survey boxes A and B. We favor thus the simple expla-

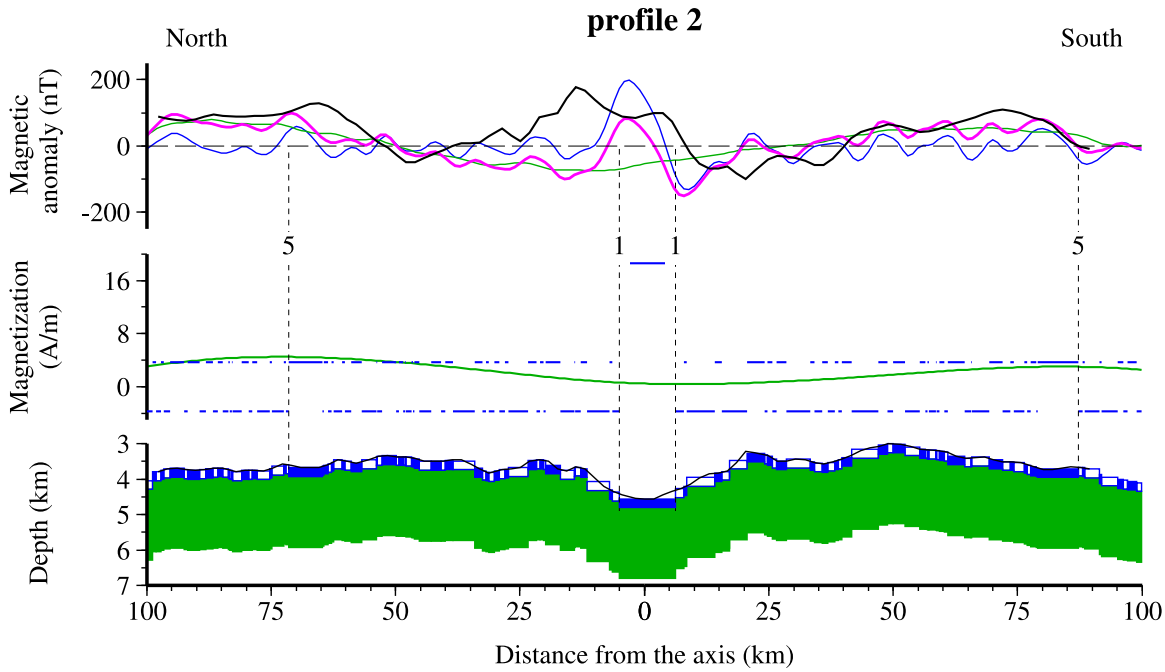

Figure 11. Forward models for profile 2 in the nontransform discontinuity between segments #20–21. Observed magnetic anomaly data are shown in black (see location of profile 2 in Figure 2). The synthetic magnetic anomaly profile shown in blue is calculated from a two-dimensional block model with a 14.5 km/m.y. spreading rates and 10% asymmetry to the south. We assume a 250 m thick magnetic layer draped on the bathymetry with a 20 A/m magnetization for the Brunhes period and a ±4 A/m magnetization off-axis. The synthetic magnetic anomaly profile shown in green is calculated assuming an induced magnetization of a 2 km thick deeper layer. This magnetization increases from 0 from the axis to 4–5 A/m at A5 time. The synthetic magnetic anomaly profile shown in magenta results from the addition of both shallow and deep contributions.

nation that the along-axis variations of the magnetization are mainly related to the size of the axial offsets. We suggest that the size of the axial offsets controls the along-axis distribution of the melt in the crust. The larger the offset, the less melt may reach the deepest part of the NTDs resulting in thinner extrusive lavas. This along-axis thickness variation of the extrusive lavas may then in turn control the along-axis magnetization variations by thinning the magnetic source layer (Figure 12).

[24] In contrast with the SWIR, crustal magnetization along slow-spreading ridges is usually described to be weakest at segment midpoints while segment ends has relatively higher magnetization [*Pockalny et al.*, 1995; *Pariso et al.*, 1996; *Ravilly et al.*, 1998; *Tivey and Tucholke*, 1998]. However, the deepest part of the NTDs was generally excluded from the magnetic studies of the MAR which have been focused on the variability in crustal magnetization along segments [e.g., *Ravilly et al.*, 1998]. We have redrawn the variation of the magnetization along the axis of the MAR between 33°–34°S and 28°30′–30°N using the magnetization solutions of *Weiland et al.* [1996] and *Pariso et al.* [1996], respectively, and including all the NTDs which were previously excluded (Figure 13). Weak magnetization is found within the NTDs in the same way as on the SWIR. The resemblance is remarkable for the largest NTD at 33°30′S (Figure 13a). The reason why little attention was paid to the magnetization in the NTDs of the MAR up to now might be related to their small size compared to the largest NTDs of the SWIR. On the MAR, segments are generally much longer than NTDs whereas on the SWIR it is the opposite. Magnetization in small NTDs may be affected by three-dimensional effects like those produced by overlapping neovolcanic zones or en echelon volcanic ridges whereas these

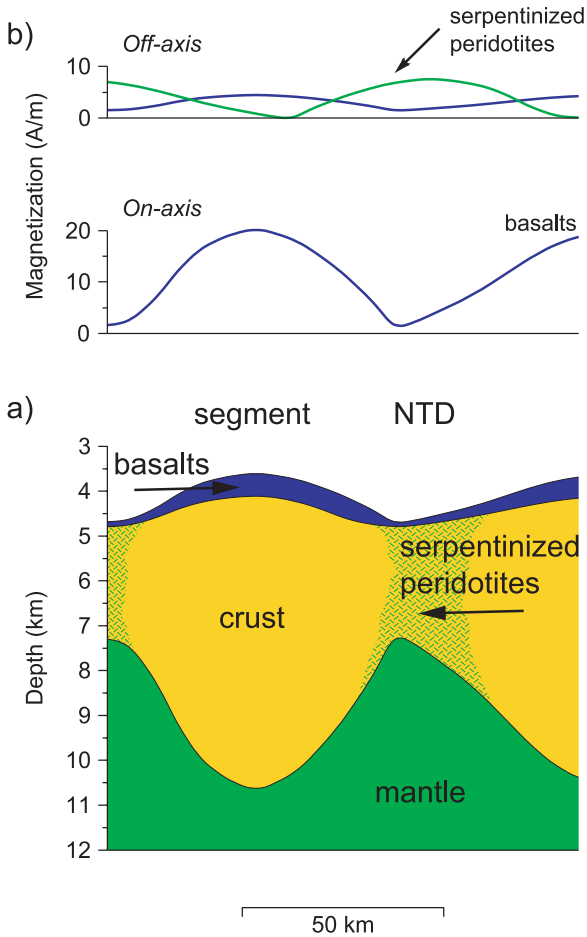

Figure 12. Schematic illustration summarizing the conclusions from this study regarding the contribution of basalts and serpentinized peridotites to marine magnetic anomalies. (a) Model for axial crust and upper mantle. The thickness of the basaltic layer decreases from 500 m on top of the segment to 100 m in the NTDs. Serpentinized peridotites outcrop in the NTDs. Thickness variations of the crust are deduced from gravity data. (b) Magnetization expected along axis and off-axis. The basaltic layer is the main magnetic source on the axis. Axial magnetization results from thickness variation of the basaltic layer. Both basalts and serpentinized peridotites produce the magnetization variations for along-isochron profiles off-axis. The remanent magnetization of the basalts has decayed significantly while an induced magnetization component has increased due to the increasing degree of serpentinization of the upper mantle rocks.

effects may be less significant in the large NTDs where the volcanic production is reduced. By contrast, a significant difference between the variation of the magnetization along the segments of the MAR and that along the segments of the SWIR is that the centers of SWIR segments are not characterized by a marked low magnetization anomaly.

6.2. No Typical Low Magnetization Anomaly at the SWIR Segment Centers

[25] Among all the segments of the three survey boxes, only the magnetization variation along segment #27, and in a much lesser extent along segments #28 and #21, looks similar to the along-axis variations of the MAR segments where magnetization is found to be weakest at segment centers and higher at segment ends. Similarly, no low magnetization anomaly was observed to the east of survey box A on two segments located between Atlantis II and Novara TFs [*Hosford et al.*, 2003]. Interpreting the length, axial relief and variation of the MBA of segment #27 in terms of magma supply and thermal structure leads to classify this segment like the segments of the MAR associated with a robust magmatic activity [*Thibaud et al.*, 1998]. The magnetization variations at these magmatically robust segments of the MAR have been explained by hotter temperatures resulting in abundant and mixed magma upon ascent and therefore low degrees of fractionation and magnetization at segment centers and higher at segment ends [*Ravilly et al.*, 1998]. The regional thermal structure also partly controls the magnetization variation along slow-spreading ridges [*Ravilly et al.*, 1998]. The lowest magnetization portion along the Reykjanes ridge is located where the Icelandic plume front is presumably located and has been explained by low degrees of fractionation stemming from a high mantle temperature [*Lee and Searle*, 2000]. On the SWIR, the strong shallowing of the axis, the decreasing of the average MBA [*Sauter et al.*, 2001] and the higher degree of melting, deduced from $Na_{8.0}$ in basaltic glasses [*Meyzen et al.*, 2003], to the west of Gallieni TF suggest that the mantle temperature is higher in survey box B than in survey box A. A hotter mantle is consistent with the local absence of an axial valley, and the abundance of volcanic edifices in segment #27 (survey box B). Likewise, a cooler mantle thermal structure in survey box A is consistent with stronger focusing of crustal accretion processes resulting in shorter segments than in

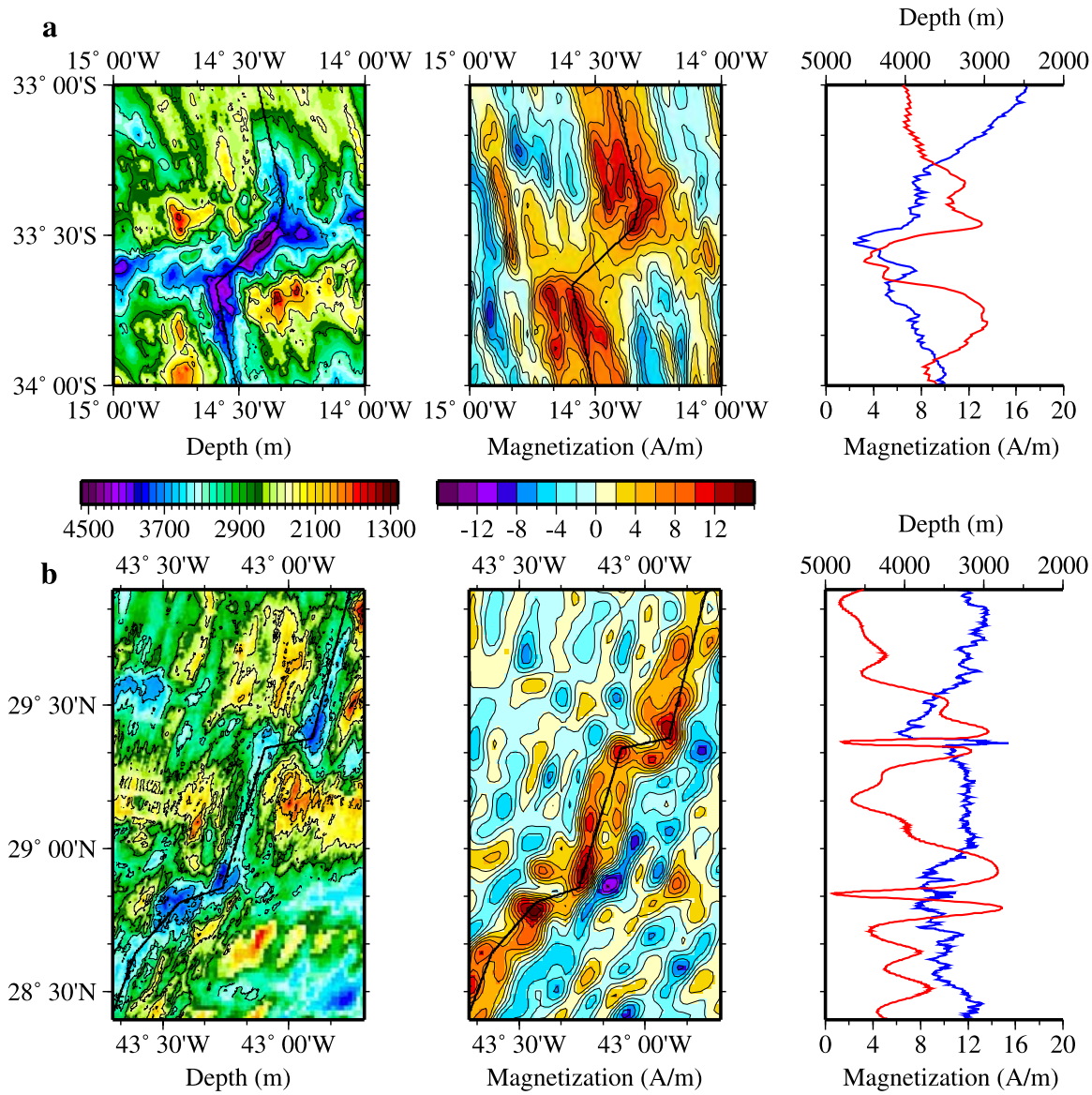

Figure 13. Magnetization distribution along two sections of the MAR. (a) Bathymetric and magnetization maps of the MAR between 33°–34°S and corresponding along-axis profiles (modified from *Weiland et al.* [1996]). (b) Bathymetric and magnetization maps of the MAR between 28°30′–30°N and corresponding along-axis profiles (modified from *Pariso et al.* [1996]). Note the weak magnetization within the NTDs.

survey box B. However, high relief segments and thick crust areas suggest that the magmatic activity is still robust in survey box A. The amplitude of the variation of MgO in basaltic glasses is much higher in survey box A (6.5–9.2%) or between Atlantis II and Novara TFs (6.1–8.8%) than in survey box B (7.3–8.6%) [*Meyzen et al.*, 2003] suggesting more frequent recharges of a magmatic reservoir in survey box B than in survey box A where the magmatic activity is thought to be more episodic leading to more evolved lavas. By contrast, the segments of survey box C show smaller crustal thickness variations, axial reliefs and seamounts density than to the west of Melville TF [*Mendel and Sauter*, 1997] suggesting a weaker magmatic activity. Survey box C is located in the deepest part of the SWIR, to the east of Melville TF, where both geophysical and geochemical data argue for a cold mantle [*Mendel et al.*, 1997; *Cannat et al.*, 1999; *Meyzen et al.*, 2003; *Seyler et al.*, 2003] resulting in

shorter lived segments [*Cannat et al.*, 2003]. We thus suggest that in segment #27 both the mantle temperature and the magmatic activity are high enough for the lavas not to be highly fractionated. A higher rate of melt production in this segment may have created some form of reservoir in the crust or in the shallow mantle, where mixing of melts occurs and where crystalline fractionation is low producing low-magnetization lavas. Although the magmatic activity is still robust at the segments of survey box A, magma chambers may be smaller in this area with cooler mantle temperatures. As a result, mixing may be restricted and significant fractionation may lead to relatively high intensity magnetization lavas even at segment centers. The weak magnetization lows of the centers of segments #28 and #21 could then reflect some intermediate stage of evolution with little more mixing and fractionation. In survey box C, both the mantle temperature and the magmatic activity are low leading to small transient magma chambers. The occurrence of low-magnetization lavas at the center of segment #27 could be tested using the empirical relationship between FeO content and NRM of *Gee and Kent* [1998]. However, only one site, among 11 in survey box B, has been dredged on this segment center. Further geochemical and paleomagnetic sampling is thus needed to test this hypothesis.

6.3. Contribution of Serpentinized Upper Mantle Rocks

[26] Higher magnetization values at segment ends at both the axis and on the flanks of the MAR were also attributed to a combination of crustal thinning and alteration of lower crust and upper mantle at segment ends [e.g., *Tivey and Tucholke*, 1998]. On the SWIR, serpentinized peridotites frequently crop out in the deepest part of the axis and therefore make up a significant portion of the lithosphere there [*Mével et al.*, 1997; *Seyler et al.*, 2003]. By contrast massive gabbros are not abundant suggesting that the composition of the upper lithosphere is mostly bimodal with volcanic and residual rocks [*Mével et al.*, 1997]. The alteration of upper mantle rocks might thus also cause an increase of the magnetization at least in the largest amagmatic sections of the SWIR. Such along-axis increase is not observed in our data which then suggests that the contribution of serpentinized upper mantle rocks to the magnetization of the axial valley is not significant (Figure 12). However, as conditions for serpentinization are most readily met in the large NTDs, where tectonic processes appear to dominate and the crust is thin or missing, upper mantle rocks may become progressively more altered as distance from the axis increases and water penetrates deeper. When peridotites reach a high degree of serpentinization (>75%), their magnetic contribution becomes significant (4–10 A/m on average) [*Oufi et al.*, 2002] and may produce the off-axis increase of the magnetization observed along the traces of the large NTDs of survey box A (Figure 12). To determine whether the induced magnetization of an upper-mantle source layer may account for this observed magnetization variation, two-dimensional forward calculations have been performed along profile 2 through the NTD between segments #20–21 (Figure 11). Because a 2–3 km thick layer interpreted to consist largely of highly serpentinized mantle rocks has been described in equivalent tectonic settings at a large 35 km nontransform offset of the MAR [*Canales et al.*, 2000], we assume a 2 km thick deep layer. The magnetization of this layer is predicted to increase from 0 at the axis to 4–5 A/m at A5 time resulting from an increasing degree of serpentinization of upper mantle rocks. The contribution of such a layer can indeed explain the long-wavelength component of the magnetic anomaly data of profile 2 (Figure 11). Strong faulting and alteration of the thin basaltic layer in the NTDs may also partly destroy the remanent magnetization of the crust [*Tivey and Tucholke*, 1998] leading to the disappearance of the magnetic reversal pattern. However, as magnetization seems to decrease after A5 time in the northernmost part of the NTDs (Figure 2d), remanent magnetization may not be completely destroyed. Further studies using longer profiles are needed to fully characterize the evolution of the magnetization along large NTDs.

[27] In the shallow axial domain of survey box B, the magnetic reversal pattern is still observed along the NTD traces which are marked, as on the MAR, by slightly more positive magnetization values

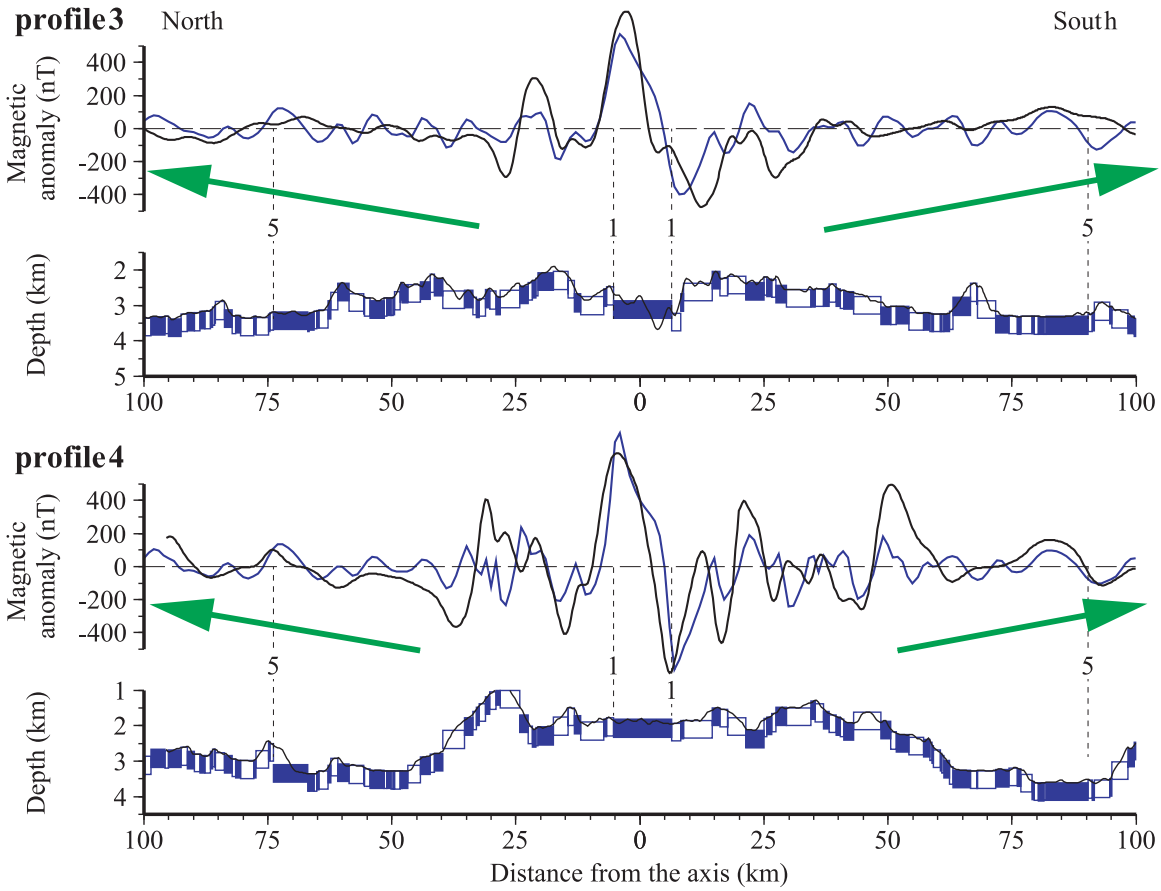

Figure 14. Forward models for profiles 3 and 4 across the shallow axial domain in survey box B. Observed magnetic anomaly data are shown in black (see location of profiles 3 and 4 in Figure 3). The synthetic magnetic anomaly profiles shown in blue are calculated from a two-dimensional block model with a 14.5 km/m.y. spreading rates and 10% asymmetry to the south. We assume a 500 m thick magnetic layer draped on the bathymetry with a 20 A/m magnetization for the Brunhes period and a ±4 A/m magnetization off-axis. Green arrows indicate the parts of the profiles where magnetization values obtained by magnetic inversion are shifted toward more positive values regardless of polarity (see Figure 9).

regardless of polarity (Figure 3d). Outside this 2–3 km thicker crust domain, there is a general shift toward more positive magnetization values regardless of polarity suggesting the presence of an induced component of magnetization (Figure 3 and 9). A long wavelength component of the magnetic anomaly data similar to that observed in the large NTDs of survey box A (Figure 11) is particularly well marked in the eastern part of survey box B where the shallow axial domain is narrower and the crust thinner than in the central part (see profile 3 in Figure 3, 9, and 14). The amplitude of the magnetic anomalies (including A5) in the outer parts of profile 3 is much lower than those predicted by forward modeling assuming a 500 m thick basaltic source layer (Figure 14). However, although subdued, the magnetic reversal pattern is not destroyed in the deeper outer part of survey box B, suggesting that the mechanism which produces more positive magnetization is weaker than in the amagmatic NTDs of survey box A. We propose that, as in these large NTDs, faulting of the thin crust areas of survey box B may facilitate the penetration of seawater down to the upper mantle rocks resulting in their weathering and an increase of their magnetization. By contrast, beneath the shallow axial domain where seawater has to cross 2–3 km thicker crust before reaching the upper mantle, the serpentinization process may be less intense and delayed. We therefore suggest that the observed shift toward more positive magnetization in the outer deeper part of survey box B

results from a contribution of serpentinized upper mantle rocks which is higher outside the shallow thicker crust domain because the shielding effect of the crust is much lower.

[28] A serpentinization process which takes 11 Ma to produce higher magnetization in the amagmatic NTDs than in the segments raises the question of the validity of the hypothesis arguing for a strong contribution of serpentinites along the present-day axis of slow-spreading ridges like the MAR [e.g., *Ravilly et al.*, 1998]. Higher magnetization values at the extremities of magmatically starved segments of the MAR might require another explanation. We thus propose that another cause, such as the presence of gabbroic intrusions at segment ends, may be responsible for the magnetization distribution along magma poor sections of the MAR. Gabbroic intrusions could be trapped at different levels in the mantle depending on the thickness of the axial lithosphere [*Cannat*, 1996; *Cannat et al.*, 1997]. The thicker the axial mantle lithosphere, the less melt should reach the crust. In the thin crust areas of the SWIR, where the effect of conductive cooling is enhanced compared to faster spreading ridges, melt may freeze at deep levels in the mantle or may migrate along the base of the lithosphere toward the segment center [*Magde et al.*, 1997]. As oceanic gabbros may have magnetization sufficient to account for sea-surface magnetic anomalies [*Worm*, 2001], shallower and larger gabbroic intrusions at slow-spreading ridges than at ultraslow-spreading ridges could thus play an important role on the along-axis magnetization distribution.

7. Conclusions

[29] The analysis of magnetic data along the SWIR suggests the following conclusions:

[30] 1. Magnetization diminishes from high values along the neovolcanic axis to low values in the axial discontinuities. There is a direct correlation between the deepening of the axial valley and the decrease of the magnetization from the extremities of the neovolcanic axis toward the deepest parts of the largest discontinuities. We suggest that less frequent eruptions as the distance from the segment center and the length of these amagmatic NTDs increase, result in thinner extrusive lavas and thus control the along-axis magnetization variations by thinning the magnetic source layer (Figure 12).

[31] 2. A unique segment centered at 50°28′E shows a marked low magnetization anomaly at its center similarly to the typical variation of the magnetization observed along the segments of the MAR. We suggest that in this segment both the mantle temperature and the magmatic activity are high enough for the lavas not to be highly fractionated. A higher rate of melt production to the west of Gallieni TF may have created some form of reservoir in the crust or in the shallow mantle, where mixing of melts occurs and where crystalline fractionation is low producing low-magnetization lavas. To the east of Gallieni TF, magma chambers may be smaller with cooler mantle temperatures resulting in restricted mixing and significant fractionation which may lead to relatively high intensity magnetization lava even at segment centers.

[32] 3. We propose that serpentinization of peridotites has no significant contribution to the variation of the magnetization along the axial valley (Figure 12). Off-axis, in thin crust areas, upper mantle rocks may become progressively more altered, as distance from the axis increases and water penetrates deeper to reach a high degree of serpentinization. The strong faulting and alteration of a thin basaltic cap and underlying upper mantle rocks can produce the disappearance of the magnetic reversal pattern and the increase of the magnetization observed along the traces of the largest NTDs of the SWIR regardless of polarity. In thick crust areas, the serpentinization process may be delayed by the shielding effect of the crust resulting, as on the MAR, in only slightly more positive magnetization values along the NTD traces, regardless of polarity.

[33] 4. A serpentinization process which takes 11 Ma to produce higher magnetization in the amagmatic NTDs than in the segments raises the question of the validity of the hypothesis arguing for a strong contribution of serpentinites along the axis of slow-spreading ridges like the MAR. Higher magnetization values at the extremities of

magmatically starved segments of the MAR might require another explanation.

Appendix A

[34] Geomagnetic storms produce irregular variations of the magnetic field resulting in large crossover errors in the magnetic anomaly data. We developed a method for removal of external variations of the magnetic field using observatory recordings and crossover analysis of magnetic profiles. We take into account the effect of errors in localization together with the effect of the observed magnetic field gradient in the neighborhood of each crossover zone.

[35] The anomaly value at data point (M, t) can be written, after correction for external field variations,

$$B_a(M,t) = F_{mes}(M,t) - B_p(M,t) - \vec{B}_v(t)\cdot\vec{f}(M) \qquad \text{(A1)}$$

where B_p is the intensity of the reference (global) field; $\vec{f}$ is the unit vector, parallel to the main field; F_{mes} is the intensity of the observed field; $\vec{B}_v$ is the field of external variations.

[36] For each observatory, the field of external variations $\vec{B}_v(Obs, t)$ can be defined as the difference between the instantaneous value of the field and its average over one month. If recordings at three surrounding observatories are available, the field of external variations in the survey area at sea can be described as the following weighted mean

$$\vec{B}_v(t) = p_1\vec{B}_v(Obs_1,t) + p_2\vec{B}_v(Obs_2,t) + p_3\vec{B}_v(Obs_3,t) \qquad \text{(A2)}$$

The parameters p_1, p_2, p_3 are calculated by inverting the following relationship

$$\delta B_a^{(i)}(\hat{C}) = \left[p_1\overrightarrow{\delta B_v}(Obs_1,t) + p_2\overrightarrow{\delta B_v}(Obs_2,t) + p_3\overrightarrow{\delta B_v}(Obs_3,t)\right]\cdot\vec{f} + x_{C_BC_A}\frac{\partial F_{mes}}{\partial x}(\hat{C}) + y_{C_BC_A}\frac{\partial F_{mes}}{\partial y}(\hat{C}) + \varepsilon \qquad \text{(A3)}$$

where $\hat{C}$ is the estimated crossover point between the two ship tracks (locally defined by segments $[A_1A_2]$ and $[B_1B_2]$), $\delta B_a^{(i)}$ is the difference between the uncorrected anomaly values at point $\hat{C}$; the $x_{C_AC_B}$ and $y_{C_AC_B}$ parameters describe for each crossover zone the deviations in the x and y directions, coming from errors in localization; ε is a random variable of zero mean.

[37] Equation (A3) can be easily generalized for a different number of observatories. In this study with N crossover points, there are $3 + 2N$ parameters. It is possible to solve this linear inverse problem by introducing a priori information through Gaussian probability laws on the data and on the parameters. This method was successfully applied to the three survey areas. The mean of the absolute value of the magnetic anomaly differences at crossover points decreases significantly from 12.8 to 6.7 nT in survey box A, from 23 to 17.6 nT in survey box B and from 12.7 to 7.6 nT in survey box C.

Acknowledgments

[38] We thank Commandant G. Tredunit, officers and crew of the R/V L'Atalante for their assistance during the Gallieni cruise. We want to thank Steve Cande, Maurice Tivey and Catherine Mével for their constructive reviews which significantly improved this manuscript. Discussions with Eric Humler and Christine Meyzen were very helpful. Thanks to Charles Weiland and Nancy Grindlay who gave us access to the data of the southern MAR. Figures were created using the public domain GMT software [*Wessel and Smith*, 1995]. This research was supported by CNRS-INSU, Géosciences Marines program. This is EOST contribution 2003.34-UMR7516.

References

Canales, J. P., R. S. Detrick, J. Lin, J. A. Collins, and D. R. Toomey (2000), Crustal and upper mantle seismic structure beneath the rift mountains and across a non-transform offset at the Mid-Atlantic Ridge (35°N), *J. Geophys. Res.*, *105*, 2699–2719.

Cande, S. C., and D. V. Kent (1995), Revised calibration of the geomagnetic polarity timescale for the Late Cretaceous and Cenozoic, *J. Geophys. Res.*, *97*, 13,917–13,951.

Cannat, M. (1996), How thick is the magmatic crust at slow spreading oceanic ridges, *J. Geophys. Res.*, *101*, 2847–2857.

Cannat, M., F. Chatin, H. Whitechurch, and G. Ceuleneer (1997), Gabbroic rocks trapped in the upper mantle at the Mid-Atlantic Ridge, *Proc. Ocean Drill. Program Sci. Results*, *153*, 243–264.

Cannat, M., C. Rommevaux-Jestin, D. Sauter, C. Deplus, and V. Mendel (1999), Formation of the axial relief at the very slow spreading Southwest Indian Ridge (49° to 69°E), *J. Geophys. Res.*, *104*, 2825–2843.

Cannat, M., C. Rommevaux-Jestin, and H. Fujimoto (2003), Melt supply variations to a magma-poor ultra-slow spreading ridge (Southwest Indian Ridge 61° to 69°E), *Geochem. Geophys. Geosyst.*, *4*(8), 9104, doi:10.1029/2002GC000480.

Chu, D., and R. G. Gordon (1999), Evidence for motion between Nubia and Somalia along the Southwest Indian Ridge, *Nature*, *398*, 64–67.

Collette, B. J., K. Rutten, H. Schouten, and A. P. Slootweg (1974), Structure of the Mid-Atlantic Ridge province between 12°N and 18°N, *Mar. Geophys. Res.*, *2*, 143–149.

Dick, H. J. B., H. Schouten, P. S. Meyer, D. G. Gallo, H. Bergh, R. Tyce, P. Patriat, K. T. M. Johnson, J. Snow, and A. Fischer (1991), Tectonic evolution of the Atlantis II fracture zone, *Proc. Ocean Drill. Program Sci. Results*, *118*, 359–398.

Dick, H. J. B., J. Lin, and H. Schouten (2003), An ultraslow-spreading class of ocean ridge, *Nature*, *426*, 405–412.

Gee, J., and D. V. Kent (1998), Magnetic telechemistry and magmatic segmentation on the southern East Pacific Rise, *Earth Planet. Sci. Lett.*, *164*, 379–385.

Grindlay, N. R., P. J. Fox, and P. R. Vogt (1992), Morphology and tectonics of the Mid-Atlantic Ridge (25°–27°30′S) from Sea Beam and magnetic data, *J. Geophys. Res.*, *97*, 6983–7010.

Hosford, A., M. Tivey, T. Matsumoto, H. Dick, H. Shouten, and H. Kinoshita (2003), Crustal magnetization and accretion at the Southwest Indian Ridge near the Atlantis II fracture zone, 0–25 Ma, *J. Geophys. Res.*, *108*(B3), 2169, doi:10.1029/2001JB000604.

Humler, E., et al. (2001), Campagne SWIFT sur la dorsale Sud Ouest Indienne entre 30°E et 50°E (N. O. Marion Dufresne, du 14 février au 21 mars 2001), Caractérisation géophysique et géochimique, *Lett. Dorsales*, *8/1–2*, 10–14.

Kuo, B. Y., and D. W. Forsyth (1988), Gravity anomalies of the ridge transform system in the South Atlantic between 31_ and 34.5_S: Upwelling centers and variation in crustal thickness, *Mar. Geophys. Res.*, *10*, 205–232.

Lee, S.-M., and R. Searle (2000), Crustal magnetization of the Reykjanes ridge and implications for its along-axis variability and the formation of axial volcanic ridges, *J. Geophys. Res.*, *105*, 5907–5930.

Macdonald, K. C. (1977), Near-bottom magnetic anomalies, asymmetric spreading, oblique spreading and tectonics of the Mid-Atlantic Ridge near 37°N, *Geol. Soc. Am. Bull.*, *88*, 541–555.

Macdonald, K. C., S. P. Miller, S. P. Huestis, and F. N. Spiess (1980), Three-dimensional modelling of a magnetic reversal boundary from inversion of deep-tow measurements, *J. Geophys. Res.*, *85*, 3670–3680.

Macmillan, S., et al. (2003), Ninth generation international geomagnetic reference field released, *Eos Trans. AGU*, *84*(46), 503.

Magde, L. S., D. W. Sparks, and R. S. Detrick (1997), The relationship between buoyant mantle flow, melt migration, and gravity bull's eyes at the Mid-Atlantic Ridge between 33°N and 35°N, *Earth Planet. Sci. Lett.*, *148*, 59–67.

Mendel, V., D. Sauter, L. M. Parson, and J.-R. Vanney (1997), Segmentation and morphotectonic variations along a super slow-spreading center: The Southwest Indian Ridge (57°E–70°E), *Mar. Geophys. Res.*, *19*, 505–533.

Mendel, V., D. Sauter, C. Rommevaux-Jestin, P. Patriat, F. Lefebvre, and L. M. Parson (2003), Magmato-Tectonic Cyclicity at the Ultra-Slow Spreading Southwest Indian Ridge: Evidence from Variations of Axial Volcanic Ridge Morphology and Abyssal Hills Pattern, *Geochem. Geophys. Geosyst.*, *4*(5), 9102, doi:10.1029/2002GC000417.

Mével, C., et al. (1997), Sampling the Southwest Indian Ridge: First results of the EDUL cruise (R/V Marion Dufresne II, August 997), *InterRidge News*, *6*, 25–26.

Meyzen, C. M., M. J. Toplis, E. Humler, J. N. Ludden, and C. Mével (2003), A major discontinuity in mantle composition beneath the Southwest Indian Ridge, *Nature*, *421*, 731–733.

Muller, M. R., T. A. Minshull, and R. S. White (1999), Segmentation and melt supply on the Southwest Indian Ridge, *Geology*, *27*, 867–870.

Munschy, M., and R. Schlich (1990), Etude géophysique des dorsales de l'océan Indien dans la région du point triple de Rodriguez, *Oceanol. Acta*, *10*, 119–128.

Oufi, O., M. Cannat, and H. Horen (2002), Magnetic properties of variably serpentinized abyssal peridotites, *J. Geophys. Res.*, *107*(B5), 2095, doi:10.1029/2001JB000549.

Pariso, J. E., C. Rommevaux, and J.-C. Sempéré (1996), Three-dimensional inversion of marine magnetic anomalies: Implications for crustal accretion along the Mid-Atlantic Ridge (28°–31°30′N), *Mar. Geophys. Res.*, *18*, 85–101.

Parker, R. L., and S. P. Huestis (1974), The inversion of magnetic anomalies in the presence of topography, *J. Geophys. Res.*, *79*, 1587–1593.

Patriat, P., and J. Ségoufin (1988), Reconstruction of the Central Indian Ocean, *Tectonophysics*, *155*, 211–234.

Patriat, P., D. Sauter, M. Munschy, and L. M. Parson (1997), A survey of the Southwest Indian Ridge axis between the Atlantis II FZ and the Indian Ocean Triple Junction: Regional setting and large scale segmentation, *Mar. Geophys. Res.*, *19*, 457–478.

Pockalny, R. A., A. Smith, and P. Gente (1995), Spatial and temporal variability of crustal magnetization of a slowly spreading ridge: Mid-Atlantic Ridge (20°–24°N), *Mar. Geophys. Res.*, *17*, 301–320.

Ravilly, M., J. Dyment, P. Gente, and R. Thibaud (1998), Axial magnetic anomaly amplitude along the Mid-Atlantic Ridge between 20°N and 40°N, *J. Geophys. Res.*, *103*, 24,201–24,222.

Robinson, C. J., R. S. White, M. J. Bickle, and T. A. Minshull (1996), Restricted melting under the very slow-spreading Southwest Indian Ridge, in *Tectonic, Magmatic, Hydrothermal and Biological Segmentation of Mid-Ocean Ridges*, edited by C. J. MacLeod, P. A. Tyler, and C. L. Walker, *Geol. Soc. Spec. Publ.*, *118*, 131–141.

Rommevaux, C., C. Deplus, and P. Patriat (1994), Three-dimensional gravity study of the Mid- Atlantic Ridge: Evolution of the segmentation between 28° and 29°N during the last 10 m.y., *J. Geophys. Res.*, *99*, 3015–3029.

Rommevaux-Jestin, C., C. Deplus, and P. Patriat (1997), Mantle Bouguer Anomaly along a super-slow spreading ridge: Comparison with the central Mid-Atlantic Ridge and implications on the accretionary process, *Mar. Geophys. Res.*, *19*, 479–501.

Sauter, D., and V. Mendel (1997), Variations of backscatter strength along the super slow-spreading Southwest indian Ridge between 57°E and 70°E, *Mar. Geol.*, *140*, 237–248.

Sauter, D., P. Patriat, C. Rommevaux-Jestin, M. Cannat, and A. Briais (2001), The Southwest Indian Ridge between 49°15′E and 57°E: Focused accretion and magma redistribution, *Earth Planet. Sci. Lett.*, *192*, 303–317.

Schouten, H., M. A. Tivey, D. J. Fornari, and J. R. Cochran (1999), Central anomaly magnetization high: Constraints on the volcanic construction and architecture of seismic layer 2A at a fast-spreading mid-ocean ridge, the EPR at 9°30′–50′N, *Earth Planet. Sci. Lett.*, *169*, 37–50.

Sempéré, J.-C. (1991), High magnetization near spreading centers discontinuities, *Earth Planet. Sci. Lett.*, *107*, 389–405.

Seyler, M., M. Cannat, and C. Mével (2003), Evidence for major-element heterogeneity in the mantle source of abyssal peridotites from the Southwest Indian Ridge (52° to 68°E), *Geochem. Geophys. Geosyst.*, *4*(2), 9101, doi:10.1029/2002GC000305.

Sichler, B., and R. Hékinian (2002), Three-dimensional inversion of marine magnetic anomalies on the equatorial Atlantic Ridge (St. Paul Fracture Zone): Delayed magnetization in a magmatically starved spreading center?, *J. Geophys. Res.*, *107*(B12), 2347, doi:10.1029/2001JB000401.

Smith, W. H. F., and D. T. Sandwell (1995), Marine gravity field from declassified Geosat and ERS-1 altimetry, *Eos Trans. AGU*, *76*, 156.

Smith, W. H. F., and P. Wessel (1990), Gridding with continuous curvature splines in tension, *Geophysics*, *55*, 293–295.

Thibaud, R., P. Gente, and M. Maia (1998), Systematic analysis of the Mid-Atlantic Ridge morphology and gravity between 15°N and 40°N: Constraints of the thermal structure, *J. Geophys. Res.*, *103*, 24,223–24,243.

Tivey, M. A., and H. P. Johnson (1987), The central magnetic anomaly high: Implications for oceanic crust construction and evolution, *J. Geophys. Res.*, *92*, 12,685–12,694.

Tivey, M. A., and B. E. Tucholke (1998), Magnetization of 0–29 Ma ocean crust on the Mid-Atlantic ridge, 25°30 to 27°10′N, *J. Geophys. Res.*, *103*, 17,807–17,826.

Tolstoy, M., A. J. Harding, and J. A. Orcutt (1993), Crustal structure on the Mid-Atlantic Ridge: Bull's-eye gravity anomalies and focused accretion, *Science*, *262*, 726–729.

Weiland, C. M., K. C. Macdonald, and N. Grindlay (1996), Ridge segmentation and the magnetic structure of the Southern Mid-Atlantic Ridge 26°S and 31°–35°S: Implications for magmatic processes at slow-spreading centers, *J. Geophys. Res.*, *101*, 8055–8073.

Wessel, P., and W. H. F. Smith (1995), New version of Generic Mapping Tools released, *Eos Trans. AGU*, *76*(29), 329.

Worm, H. U. (2001), Magnetic stability of oceanic gabbros from ODP Hole 735B, *Earth Planet. Sci. Lett.*, *193*, 287–302.

Zhou, W., R. Van der Voo, D. R. Peacor, D. Wang, and Y. Zhang (2001), Low-temperature oxidation in MORB of titanomagnetite and titanomaghemite: A gradual process with implications for marine magnetic anomaly amplitudes, *J. Geophys. Res.*, *106*, 6409–6421.